HHS Public Access

Author manuscript

Cell Stem Cell. Author manuscript; available in PMC 2024 November 02.

Published in final edited form as:

Cell Stem Cell. 2023 November 02; 30(11): 1503–1519.e8. doi:10.1016/j.stem.2023.09.011.

SRCAP Mutations Drive Clonal Hematopoiesis Through Epigenetic and DNA Repair Dysregulation

Chun-Wei Chen[1,2,3], **Linda Zhang**[2,3,4,5], **Ravi Dutta**[6], **Abhishek Niroula**[7,8], **Peter G. Miller**[6,9], **Christopher J. Gibson**[7], **Alexander G Bick**[6,10], **Jaime M. Reyes**[2,3], **Yi-Tang Lee**[1,11], **Ayala Tovy**[2,3], **Tianpeng Gu**[2,3], **Sarah Waldvogel**[2,3,5], **Yi-Hung Chen**[2], **Bryan J. Venters**[12], **Pierre-Olivier Estève**[13], **Sriharsa Pradhan**[13], **Michael-Christopher Keogh**[12], **Pradeep Natarajan**[6,14,15], **Koichi Takahashi**[16], **Adam S. Sperling**[6,7,8], **Margaret A. Goodell**[2,3,5,17]

[1.]Interdepartmental program in Integrative Molecular and Biomedical Sciences, Baylor College of Medicine, Houston, Texas, USA

[2.]Department of Molecular and Cellular Biology, Baylor College of Medicine, Houston, Texas, USA

[3.]Stem Cells and Regenerative Medicine Center, Baylor College of Medicine, Houston, Texas, USA

[4.]Program in Translational Biology and Molecular Medicine, Houston, Texas, USA

[5.]Medical Scientist Training Program, Baylor College of Medicine, Houston, TX, USA

[6.]Division of Hematology, Brigham and Women's Hospital, Boston, MA, USA

[7.]Broad Institute of MIT and Harvard, Cambridge, MA, USA

[8.]Department of Medical Oncology, Dana-Farber Cancer Institute, Boston, MA, USA

[9.]Center for Cancer Research and Center for Regenerative Medicine, Massachusetts General Hospital, Boston, MA

[10.]Division of Genetic Medicine, Department of Medicine, Vanderbilt University Medical Center, Nashville, TN, USA

[11.]Department of Molecular and Human Genetics, Baylor College of Medicine, Houston, Texas, USA

[12.]EpiCypher Inc., Durham, NC, USA

[13.]New England Biolabs, Ipswich, MA, USA

[14.]Cardiovascular Research Center, Massachusetts General Hospital, Boston, MA, USA

[*]Correspondence: goodell@bcm.edu.

Authors Contributions

Conceptualization: C.W.C, L.Z., and M.A.G; formal analysis and data curation: C.W.C; investigation: C.W.C, L.Z., R.D. A.N., Y.L., Y.C, A.S.S; methodology: C.W.C, J.M.R, A.T., T.G., S.W., B.J.V, P.O.E., S.P., M.C.K.; resources: R.D., P.G.M, C.J.G, A.G.B., P.N., K.T., and A.S.S; writing – original draft: C.W.C and M.A.G; writing – review & editing: L.Z., B.J.V, M.C.K, A.S.S, and M.A.C; supervision: C.W.C, A.S.S, and M.A.G.

[15]Department of Medicine, Harvard Medical School, Boston, MA, USA

[16]Department of Leukemia, The University of Texas MD Anderson Cancer Center

[17]Lead contact

Summary

Somatic mutations accumulate in all cells with age and can confer a selective advantage, leading to clonal expansion over time. In hematopoietic cells, mutations in a subset of genes regulating DNA repair or epigenetics frequently lead to clonal hematopoiesis. Here we describe the context and mechanisms that lead to enrichment of hematopoietic stem cells with mutations in *SRCAP*, which encodes a chromatin remodeler that also influences DNA repair. We show that *SRCAP* mutations confer a selective advantage in human cells and in mice upon treatment with the anthracycline-class chemotherapeutic doxorubicin and bone marrow transplantation. Furthermore, *Srcap* mutations lead to a lymphoid-biased expansion, driven by loss of SRCAP-regulated H2A.Z deposition and increased DNA repair. Altogether, we demonstrate that SRCAP operates at the intersection of multiple pathways in stem and progenitor cells, offering a new perspective on the functional impact of genetic variants that promote stem cell competition in the hematopoietic system.

Graphical Abstract

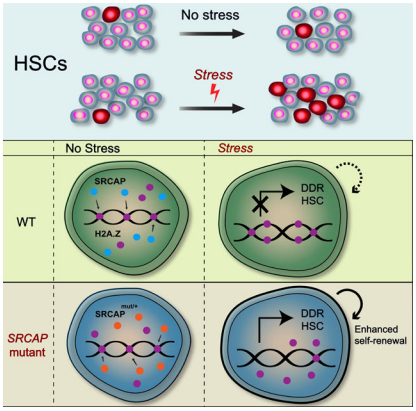

eTOC Blurb:

Chen and colleagues demonstrate that mutations in the chromatin remodeler SRCAP are recurrently found in clonal hematopoiesis, particularly after genotoxic exposure. Modeling reveals mutant cell advantage is triggered by stress and driven by enhanced stem cell function. Augmented epigenetic regulation with DNA damage repair reveal new mechanisms promoting clonal hematopoiesis.

Keywords

clonal hematopoiesis; lymphoid; SRCAP; hematopoietic stem cells; chromatin remodeling; H2A.Z; DNA damage

Introduction

Mutations steadily accumulate in all somatic cells throughout life.[1] Some somatic mutations confer a selective advantage such that the mutant cell and its progeny outcompete other cells within a tissue, forming an expanded clone. This ultimately leads to somatic mosaicism, a process that is now recognized to be universal across all tissue types and that increases with age.[2] Clonal hematopoiesis (CH) is one case of such competition within the blood.[3] In CH, hematopoietic stem cells (HSCs) acquire somatic mutations that confer selective advantages, leading to clonal expansion of variant HSCs and their progeny.[4] CH increases with age and is ubiquitously found in elderly individuals.[5] The development of CH can be accompanied by a lymphoid or myeloid lineage bias,[6] affecting downstream peripheral blood production, and is associated with an increased risk of hematologic malignancy.[7]

Recurrent CH gene mutations can be broadly grouped into several functional classes. Epigenetic modifiers, such as *DNMT3A* and *TET2*, form the largest class. Mutations in these genes drive clonal expansion through intrinsic regulation of epigenetic landscape.[8–10] These mutations confer mutant HSCs with enhanced stem cell self-renewal capacity due to dysregulation of the cellular epigenetic landscape.[11] Another major class of genes recurrently found in CH includes several involve in DNA damage repair (DDR), such as *TP53* and *PPM1D*, where mutant HSCs show increased survival under stress. While such expanded clones can be found in all large studies,[12–15] they are highly enriched under certain contexts. For example, *PPM1D* mutations are prevalent in individuals who have had prior exposure to the platinum chemotherapeutic agent cisplatin.[16,17] Some of these CH drivers, such as *TP53*, are associated with higher risk of malignancy development and a poor long-term prognosis.[13,18] Therefore, it is not only important to identify CH driver genes, but also the context in which they are relevant.

While the above classifications of CH genes have been useful to begin to understand the phenomenon, discrete categorization ignores overlap in their functional impact. For example, while *DNMT3A* mutations are thought to confer enhanced stem cell self-renewal primarily through the role of this DNA methyltransferase in epigenetic regulation,[19–21] enhanced DDR has also been observed with the DNMT3A^{R882} mutant.[22] Similarly, clonal advantage of *TP53* mutants may be influenced by epigenetic regulation in addition to their canonical effects on DDR.[23] Therefore, to better understand the mechanisms driving CH, it is critical to interrogate multiple facets of the functional potential of CH-associated variants.

Mutations in a few genes such as *DNMT3A* and *TET2* account for the majority of cases of CH with identifiable drivers, but there is a sizable number of genes in which mutations are observed less frequently, and which collectively contribute to a large proportion of CH. Understanding the role played by these genes in regulating stem cell fitness and clonal expansion may lend insight into hematopoiesis, broadly, as well as aging and cancer. We became interested in an understudied gene, *SRCAP* (encoding Snf2-related CREBBP activator protein), which has appeared in CH in multiple studies.[14,15,24,25]

SRCAP is a CREB-binding protein that encodes the core catalytic ATPase component of the chromatin remodeling SRCAP complex.[26] This complex is important for introducing

the histone H2A variant, H2A.Z, into the nucleosome, evicting canonical H2A.[27] H2A.Z is important for gene regulation, epigenetic modification, and mammalian development.[27–30] The introduction of H2A.Z decreases chromatin accessibility and negatively regulates gene expression.[31–34] Interestingly, SRCAP has also been implicated in the DDR. SRCAP is recruited to the site of DNA double-stranded breaks[29] and promotes homologous recombination.[35] Thus, SRCAP is associated with epigenetic regulation and the DDR, both of which are implicated in CH. However, little is known about the role of SRCAP in hematopoiesis and stem cell function, whether *SRCAP* mutations are selected under certain conditions, and which pathways are relevant.

Here, we analyzed human CH data to study the context in which *SRCAP* mutations are relevant and generated a *Srcap* mutant mouse model to demonstrate a role for the enzyme in modulating the chromatin landscape and gene expression. Understanding how *SRCAP* mutations in CH offered an opportunity to examine the potential contribution of different functional aspects in the development of CH.

Result

CH-associated *SRCAP* mutations are enriched following exposure to genotoxic agents

In order to determine the distribution of *SRCAP* mutations in humans, we collected data from twelve independent clinical studies of both healthy individuals and those with a cancer diagnosis[14,15,24,25]; these studies harbored 367 *SRCAP* mutations. In addition to the UK and Mass General Brigham (MGB) Biobanks, which primarily include individuals without a cancer diagnosis, these cohorts include a diverse set of patients with malignant diagnoses including multiple myeloma (MM), non-Hodgkin lymphoma (NHL),[15,24] myelodysplastic syndromes (MDS), acute myeloid leukemia (AML),[36,37] chronic lymphocytic leukemia (CLL),[38] melanoma,[39] and breast cancer[40] many of whom have been previously exposed to anti-cancer therapies (Figure 1A).

Since *SRCAP* CH has not been extensively studied, we assessed the age-dependency and sex bias by analyzing individuals in the UK Biobank cohort where sex and age information are available. The prevalence of *SRCAP* mutations increases with age and is higher in females (n=95) over males (n=46) (Figure 1B). In a multivariable logistic regression model adjusting for age and smoking status, the odds ratio for *SRCAP* mutations in females was 1.71 (95% confidence interval = 1.2 – 2.44, p=0.0028). In addition, an identical analysis with MGB Biobank cohort showed similar age-dependent increase in occurrence with a trend towards a female bias (Figure S1A). This observation suggests a potential sex-specific selection for *SRCAP* mutations.

Importantly, in several of the cancer cohorts (MM, NHL, melanoma, and breast cancer), sequencing was performed from peripheral blood samples and thus the *SRCAP* mutations are not in the tumor cells representing CH. In addition, these patients were sequenced with the same NGS panel allowing for direct comparison. Because patients are typically treated with multi-agent chemotherapy, we stratify the patients into two cohorts based on their history of exposure to genotoxic chemotherapy to determine whether *SRCAP* mutations are enriched following exposures. We compared the prevalence of *SRCAP* mutations in

two cohorts of patients: MM or NHL patients heavily exposed to (chemo-exposed) and melanoma patients without exposure to (chemo-naïve) genotoxic therapy. We found a significant enrichment of *SRCAP* mutations, as well as for mutations in other genes that regulate the DNA damage response including *PPM1D* and *TP53*, in the chemo-exposed cohort (Figure 1C). When we included mutations with a VAF less than 0.01, the difference was even more significant (14% vs 3%, $p<0.0001$). We conclude that *SRCAP* mutations are enriched in individuals exposed to cellular genotoxic stress.

With many known functional domains of the SRCAP protein, we plotted the distribution of 367 *SRCAP* mutations and found that, while *SRCAP* mutations occur across the entire length of the gene, nonsense and frameshift mutations were enriched at the region close to the CREB-binding protein (CBP) interaction domain (Figure 1D). To determine whether exposure to cellular stress shapes the spectrum of *SRCAP* mutations, we compared the distribution of *SRCAP* mutations in patients with (n=86) and without (n=269) prior exposure to genotoxic therapy. We found no notable difference in the distribution (Figure S1B). This suggests that genotoxic exposure does not cause *SRCAP* mutations but selects the fitness of *SRCAP* mutants. Based on all the clinical cohorts collected, we then assessed the importance of *SRCAP* mutations clustering at the region close to CBP-binding domain by examining the structure of SRCAP chromatin remodeling complex[26] (PDB 6IGM, Figure 1E). This analysis shows that the CH-enriched region is located where SRCAP interacts with the nucleosome, connecting the two lobes of SRCAP (Figure S1C). This implicates that this region may play a pivotal role in SRCAP function. We therefore hypothesize that nonsense mutations in the CH-enriched region lead to a truncated SRCAP protein which impacts hematopoiesis and potentially confers a competitive advantage on HSCs.

Increased clonal expansion of *SRCAP* mutant cells following genotoxic stress

To investigate the impact of *SRCAP* mutations on clonal hematopoiesis, we modeled a recurrent CH-associated mutation in human cells. We generated a truncating mutation at residue 1963 (Q1963* in exon 26) using CRISPR-Cas9 and homology-based DNA repair, simultaneously inserting a C-terminal FLAG tag (Figure S1D) in human leukemia MOLM-13 cells (hereafter *SRCAP*$^{mut/+}$) (Figure S1E). To verify expression of WT and mutant alleles, we examined their mRNA expression in WT and *SRCAP*$^{mut/+}$ MOLM-13 cells with allele-specific RT-qPCR primers. While only WT was expressed in the WT cells, both WT and mutant alleles were present in *SRCAP*$^{mut/+}$ cells (Figure S1F). This verified that the *SRCAP* mutant allele is expressed at least at the RNA level and has the potential to generate a truncated protein.

Due to the enrichment of *SRCAP* CH-mutations in individuals treated with chemotherapeutic agents, often with combinations of multiple agents, it is critical to understand specific contexts that enhance the selective advantage of *SRCAP* mutant cells. We tested the response of *SRCAP*$^{mut/+}$ cells to various classes of frequently used cytotoxic agents with different mechanisms of action. First, we established dose-response curves at baseline or treated with other cytotoxic drugs, including doxorubicin, etoposide, and cytarabine (Figure 2A and S2A), and observed that *SRCAP*$^{mut/+}$ cells were specifically more resistant to doxorubicin with a significantly higher IC50. The drug specificity towards

doxorubicin was recapitulated in K562 leukemia cells and mouse embryonic fibroblasts (MEFs), which represent healthy cells with a defined genetic background (Figure S2B).

Next, we determined the cellular responses leading to such drug specificity. In the apoptosis assay, *SRCAP*$^{mut/+}$ cells demonstrated an increased proportion of viable cells and a decreased proportion of apoptotic cells after doxorubicin treatment (Figure 2B and S2C). While a slight decrease in apoptosis was also observed in *SRCAP*$^{mut/+}$ cells treated with etoposide, treatment with cytarabine did not induce a differential apoptotic response between WT and mutant cells (Figure S2D).

Doxorubicin is known to cause cell cycle arrest at the G2/M phase, so we used BrdU to examine the effect of the *SRCAP* mutation on cell cycle progression. Strikingly, *SRCAP*$^{mut/+}$ cells were more resistant to doxorubicin-induced G2/M arrest and maintained an unaltered cell cycle distribution before and after treatment (Figure 2C). The resistance to G2/M arrest was the most dramatic with doxorubicin compared to other chemotherapeutic agents (Figure S2E). The data suggest that the differential responses between WT and *SRCAP*$^{mut/+}$ cells may be specific to particular classes of drugs, and we sought to better understand the drug specificity in the context of competition.

To assess if *SRCAP*$^{mut/+}$ cells exhibit a competitive advantage over WT cells, we competed the cells in the same mixture by generating a constitutive GFP-labeled MOLM-13 cell line using CRISPR/Cas9. The isogenic WT GFP-positive clone was clearly distinguishable from the isogenic *SRCAP*$^{mut/+}$ GFP-negative population by flow cytometry (Figure 2D). After mixing *SRCAP*$^{mut/+}$ and WT cells at 20:80, this ratio remained stable in untreated culture for at least eight days (Figure S2F), indicating no selective advantage. However, when mixed cultures were treated with doxorubicin, *SRCAP*$^{mut/+}$ MOLM-13 cells gradually outcompeted WT GFP+ cells (Figure 2D) demonstrating a drug-induced selective advantage. Such significant expansion in competition assays is consistent with the behavior of other CH-associated genes[16,17], in which a modest fitness advantage with a single exposure (Figure 2A–C) is compounded with multiple exposures, particularly over time (Figure 2D), leading to a readily discernable advantage and phenotype

The mutant cell expansion was not observed when treated with other chemotherapeutic agents (Figure S2F), indicating the anthracycline drug doxorubicin can specifically promote the fitness of *SRCAP*$^{mut/+}$ cells. This expansion phenotype was also absent in *SRCAP* heterozygous (*SRCAP*$^{+/-}$) knockout cells (Figure S2G), suggesting a neomorphic function of this *SRCAP* mutation. Together, these data demonstrate that the response of *SRCAP*$^{mut/+}$ cells is drug specific in this context, and that the fitness of *SRCAP*$^{mut/+}$ cells is selected for particularly by the anthracycline drug doxorubicin.

SRCAP mutant cells exhibit enhanced DNA damage response

Given the role of SRCAP in DDR,[35] we considered whether the selective resistance of *SRCAP*$^{mut/+}$ cells to doxorubicin was a result of differential DNA damage response, as doxorubicin intercalates into DNA and leads to adduct formation. We first determined whether there were changes in protein levels after doxorubicin treatment by utilizing MEFs. We found that there were no significant differences between endogenous SRCAP WT

(~400 kDa) and mutant (~240 kDa) protein expression at baseline or after treatment with doxorubicin (Figure 2E). Therefore, we hypothesized that *SRCAP*$^{mut/+}$ cells demonstrated selective resistance to doxorubicin due to enhanced DDR in the heterozygous state.

Since SRCAP has also been implicated in promoting homologous recombination (HR),[35] we utilized reporter cell lines to assess repair efficiency through either HR or non-homologous end joining (NHEJ) to examine DDR mechanisms leveraged by *SRCAP*$^{mut/+}$ cells. The U2OS-based HR and NHEJ reporter cell lines harbor cassettes in which DNA damage is induced by expression of I-SceI endonuclease. Successful repair through HR or NHEJ is identified by GFP expression.[41] We generated isogenic *SRCAP*$^{mut/+}$ clones in both lines using CRISPR-Cas9 (Figure S2H). We observed a significant increase in both HR and NHEJ efficiency in *SRCAP*$^{mut/+}$ cells (Figure 2F), indicating *SRCAP*$^{mut/+}$ cells leverage both repair pathways to promote cellular fitness.

Next, we assessed whether increased DDR led to selective advantage in the MOLM-13 human cell line. *SRCAP*$^{mut/+}$ MOLM-13 cells upregulated DDR genes after doxorubicin treatment (Figure 2G), consistent with increased DDR as a mechanism for the *SRCAP* fitness advantage. Finally, treatment with a PARP inhibitor, Pamiparib, which blocks the DDR, along with doxorubicin abrogated the fitness advantage of *SRCAP*$^{mut/+}$ in the cell-based competition assay (Figure 2H). This indicates that the enhanced fitness of this *SRCAP* mutant to anthracycline drugs is at least in part a result of increased DDR.

Srcap-mutant mice exhibit normal hematopoiesis in the absence of stress

To investigate the effect of *SRCAP* mutations on a normal WT genetic background *in vivo*, we generated mice bearing the same FLAG-tagged truncating mutation described above at the endogenous *Srcap* locus (Figure S1D). WT and mutant mRNA expression were confirmed by allele-specific PCR in hematopoietic stem and progenitor cells (HSPCs, defined throughout using Lin$^-$Sca1$^+$cKit$^+$ markers; see Table S3; Figure S3A). Of note, heterozygous mice bearing *Srcap*-Q1963* (hereafter *Srcap*$^{mut/+}$) were maintained in a heterozygous state with no obvious impact on their breeding or appearance. No *Srcap*$^{mut/mut}$ mice were identified indicating that the homozygous mutant state is embryonically lethal.

We next examined baseline hematopoiesis and HSC function in germline *Srcap*$^{mut/+}$ mice. We assessed the properties of bone-marrow derived long-term hematopoietic stem cells (HSCs, CD150$^+$CD48$^-$ HSPCs; see Table S3), observing that WT and *Srcap*$^{mut/+}$ HSCs showed similar cell cycle distribution, with each the population predominantly quiescent in G0/G1 phase (Figure S3B). Colony-forming capacity in each background was similar after primary and secondary plating (Figure S3C), suggesting similar proliferative capacity of HSCs. Hematopoietic lineage distribution for myeloid (CD11b$^+$Ly6C/Ly6G$^+$), B (B220$^+$), and T (CD4$^+$Cd8$^+$) cells from bone marrow and peripheral blood was also similar between WT and *Srcap*$^{mut/+}$ mice (Figure S3D). Together, this demonstrates that the CH-associated mutation does not affect normal hematopoiesis. Therefore, *SRCAP* mutants likely require cellular stressors to promote their competitive advantage in the context of CH.

Srcap$^{mut/+}$ expansion originates from HSCs

While *SRCAP* mutants are selected by genotoxic stress, most individuals have had prior exposure to cytotoxic therapeutics before transplantation. We sought to utilize the murine model to study healthy cells and determine whether transplantation is a stressor that promotes *Srcap*$^{mut/+}$ cell expansion. We mixed *Srcap*$^{mut/+}$ bone marrow cells with those from WT mice at a 10:90 ratio and transplanted them into lethally irradiated WT mice. The donor cells and their progeny can be distinguished using the CD45.1/2 allelic system (nucleated hematopoietic cells from mutant mice express CD45.2, and from the WT CD45.1; Figure 3A). A parallel transplant competing WT (CD45.2) against WT (CD45.1) cells serves as a control.

At early time points after transplantation, the *Srcap*$^{mut/+}$ cells had a similar contribution to blood production when competing with the WT cells. Interestingly, 12 weeks after the transplantation, we observed an expansion of *Srcap*$^{mut/+}$ cells in the peripheral blood of recipients that continued to increase until 20 weeks post-transplantation. These data indicate that *Srcap*$^{mut/+}$ cells exhibited a marked advantage compared to the parallel WT:WT transplant, and they generated almost 50% more progeny than WT cells 20 weeks after the transplantation (Figure 3B). Such expansion was observed in both male and female mice, indicating that the mechanism leading to the female bias is not fully recapitulated in this model. We also performed competitive transplantation with heterozygous knock-out (*Srcap*$^{+/-}$) cells and, similar to human cell lines, observed no expansion (Figure S3E), suggesting that the *Srcap* mutation is neomorphic.

We also assessed cell expansion after additional stressors. After secondary transplantation, we observed no further expansion (Figure S3F). Similarly, doxorubicin treatment after primary transplantation did not lead to further expansion (Figure S3G). These data suggest that, despite significantly increased fitness upon the primary stress, *Srcap*$^{mut/+}$ cells do not gain further advantage upon a secondary exposure, at least within the timeframes examined here. We hypothesize that the elevated DDR is accompanied by epigenetic changes which, after the altered epigenetic landscape is established during the primary exposure, *Srcap*$^{mut/+}$ cells are not subject to further alterations.

To characterize *Srcap*$^{mut/+}$ expansion in blood, we analyzed the chimerism of donor (CD45.2) cells in the bone marrow 20 weeks after transplantation. The most significant increase in *Srcap*$^{mut/+}$ chimerism was observed in the HSPC and purified HSC populations (Figure 3C–D), indicating that *Srcap* expansion originated from HSCs, accounting for the greater representation of their progeny in the peripheral blood. As CH is sometimes accompanied by a lineage bias,[7] we examined the hematopoietic lineage composition in our competitive transplant model. Strikingly, within the lineage-committed progenitors, the expansion of *Srcap*$^{mut/+}$ cells was restricted to the common lymphoid progenitors (CLPs; Figure 3E, S3H, and Table S3). In addition, we found similar absolute number of HSCs and CLPs in the bone marrow between the *Srcap*$^{mut/+}$:WT and WT:WT transplant cohorts (Figure S3I), demonstrating that the advantage of the *Srcap* mutant cells is due to a dynamic competition with WT HSCs and not aberrant outgrowth.

Importantly, we observed over-representation of *Srcap*$^{mut/+}$ cells within the B-cell population in the bone marrow, peripheral blood, and spleen (Figure 3F and S3J). In accordance, *Srcap*$^{mut/+}$ expansion occurs at 12 weeks post-transplantation (Figure S3K) and can be found in the blood, bone marrow, and spleen, which is mostly comprised of B-cells, but not in the thymus (Figure 3G), which is largely composed of T-cells. Together, these results indicate that *Srcap* expansion originates from the HSC population, and affects the downstream lymphoid lineage, ultimately contributing to B-cells. Furthermore, we demonstrate that transplantation is a cellular stressor that promotes the advantage of *Srcap*$^{mut/+}$ cells, consistent with other reports showing *SRCAP*-mutant CH.[14,24]

Transcriptomic regulation of *Srcap* lymphoid-biased expansion

To examine the mechanism through which mutations in SRCAP, a chromatin remodeler, affect *Srcap*$^{mut/+}$ expansion, we investigated the transcriptome of the hematopoietic progenitors. We performed RNA-sequencing on sorted donor (CD45.2) HSPCs from the bone marrow transplants described above (Figure 3A). We first asked whether differentially expressed genes suggested enhanced stem cell function, consistent with the competitive advantage of mutant HSCs. While no significant differences were observed pre-transplantation, after transplantation, *Srcap*$^{mut/+}$ HSPCs harbored elevated expression of genes typically found at high levels in HSCs[42] (Figure 4A–B and S4A). This indicates that the *Srcap*$^{mut/+}$ cells harbor an up-regulation of these HSC-associated genes in the context of bone marrow transplantation.

Because HSPCs are heterogeneous, we turned to single-cell RNA sequencing to examine if transcriptional changes in HSPCs from transplant recipients could explain the lymphoid-biased differentiation (Figure 4C and S4B). While we observed no significant differential abundance of cell clusters between WT and *Srcap*$^{mut/+}$ HSPCs (Figure S4C), we found that the top differentially regulated genes within the lymphoid-primed clusters were involved in cell fate commitment during hematopoiesis such as *Hoxc6*, *Cxcl10*, and *Ly6c2* (Figure S4D).

To better understand the transcriptome, we extracted the top differentially regulated gene signature found in the *Srcap*$^{mut/+}$ lymphoid cluster (Figure S4E). When scoring based on this gene signature and plotting in all clusters, we found that the *Srcap*$^{mut/+}$ signature was also up-regulated in *Srcap*$^{mut/+}$ HSCs but not in the myeloid cluster (Figure 4D). This is consistent with the *Srcap* expansion phenotype. We performed gene set enrichment analysis (GSEA) comparing *Srcap*$^{mut/+}$ to WT lymphoid clusters focusing on pathways related to hematopoiesis and the expansion. This revealed up-regulation of GO terms related to cell fate commitment and cell growth (Figure S4F). We then analyzed genes in one of the most significantly up-regulated GO terms, '*positive regulation of cell growth*' (GO:0030307). We observed significant up-regulation in '*positive regulation of cell growth*' in the *Srcap*$^{mut/+}$ lymphoid, but not the myeloid, cluster (Figure 4E). Thus, the transcriptomic analyses are consistent with a competitive advantage in *Srcap*$^{mut/+}$ HSCs and lymphoid, but not myeloid, cells, aligning with the phenotype observed in mice.

Taken together, our characterization of *Srcap* expansion demonstrates that *Srcap*$^{mut/+}$ expansion originates from HSCs, impacting downstream hematopoiesis with a lymphoid bias specifically restricted to the B-cell compartment (Figure 4F).

Srcap-mutant cell fitness is enhanced by distinct modes of stress

Data from MOLM-13 human cell line indicated anthracycline exposure led to increased selection of *SRCAP*$^{mut/+}$ over WT cells due to enhanced DDR and decreased cell cycle arrest. Similarly, data from mice indicated enhanced fitness of *Srcap*$^{mut/+}$ cells after transplantation based on up-regulation of a stem cell-related program. Genotoxic therapies[12] and transplantation[24,43] are both common stressors in the hematopoietic system. Since we reported that the advantage of *SRCAP* mutant cells was promoted by both stressors, we sought to directly compare the impact of the two cellular stressors, doxorubicin treatment and transplantation, on the competitive advantage of *Srcap*$^{mut/+}$ cells.

To compare the two cellular stressors *in vivo*, we established new mouse cohorts in which we harvested WT or *Srcap*$^{mut/+}$ HSPCs 12 hours after a single dose of doxorubicin treatment, or 2 weeks after bone marrow transplantation (the earliest possible time-point after recovery from irradiation; Figure 5A). We assessed transcriptome in response to the two stressors by performing RNA-sequencing on purified HSPCs (Figure 5A and S5A). GSEA revealed similar up-regulation of pathways related to cell cycle and DDR and down-regulation in immune response between the two cohorts (Figure 5B). While there was no difference at baseline pre-treatment, HSC genes and '*positive regulation of DNA repair*' (GO:0045739) were two of the most up-regulated pathways in *Srcap*$^{mut/+}$ HSPCs after exposure to doxorubicin or transplantation (Figure 5C and S5B-D). Interestingly, this up-regulation of DDR was also accompanied by elevated expression of genes enriched in HSCs[42] (Figure 5D). The enhanced fitness of *Srcap*$^{mut/+}$ HSPCs was functionally validated with increased colony-forming capacity (Figure S5E). This transcriptomic up-regulation in both DDR and HSC maintenance pathways suggests the involvement of SRCAP in both CH-associated functional classes, DDR and epigenetics.

We validated that transcriptional upregulation of DDR pathways was associated with a functional difference in DDR activation using a comet assay and γH2AX immunofluorescence. The induction of DDR was detectable by both techniques at 12 hours after doxorubicin and two weeks after transplantation (Figure S5F–G). We evaluated the DDR response by analyzing the tail moment of each cell in the comet assay to denote the amount of DNA damage. We observed that, after doxorubicin treatment and transplantation, *Srcap*$^{mut/+}$ HSPCs exhibited significantly lower levels of DNA damage (Figure 5E). Such decreased level of DNA damage was not found in *Srcap*$^{mut/+}$ HSPCs when treated with non-anthracycline drugs, cytarabine and etoposide (Figure S5H), indicating that the elevated DDR is specific to the anthracycline drug doxorubicin. Similarly, *Srcap*$^{mut/+}$ HSPCs showed significantly fewer γH2AX foci after doxorubicin treatment and transplantation (Figure 5F). Moreover, when we assessed the percentage of γH2AX-positive cells in HSCs, there were fewer γH2AX-positive cells in *Srcap*$^{mut/+}$ HSPCs, indicating enhanced DDR following both doxorubicin and transplantation as stress mechanisms (Figure 5G and S5I-J).

Finally, to validate that increased DDR was associated with the expansion phenotype, we assessed the transcriptome of downstream lineage populations by performing RNA-sequencing in B and T cells isolated from the bone marrow after transplantation. We found the up-regulation of gene set "*positive regulation of DNA repair*" in the B- but not T-cells (Figure 5H), indicating that the transcriptomic up-regulation of DDR was associated with *Srcap* expansion and the lineage bias observed at the phenotypic level.

Taken together, these data show that distinct cellular stressors, doxorubicin treatment and bone marrow transplantation, lead to similar DDR and transcriptional changes in *Srcap*$^{mut/+}$ stem cells, indicating that exposure to the two stressors potentially promotes *Srcap* expansion through the same mechanism. Since gene expression patterns are linked to epigenetic landscape, and given SRCAP's role in chromatin remodeling, we considered the broader role of SRCAP in epigenetic regulation.

Decreased chromatin remodeling of *Srcap* mutant cells after stress

SRCAP remodels chromatin by incorporating histone variant, H2A.Z, into the nucleosome; and H2A.Z at promoters can affect gene expression.[27,29] A role for SRCAP and H2A.Z has not been investigated in blood; therefore, we assessed whether the epigenetic landscape is linked to transcriptomic regulation as a mechanism leading to enhanced fitness. RNA-sequencing data generated after transplantation revealed decreased chromatin remodeling (GO:0006338) capacity (Figure 5B), indicating that the differential chromatin landscape may be associated with the competitive advantage of mutant cells.

To test this hypothesis, we examined SRCAP chromatin remodeling activity and SRCAP-regulated H2A.Z deposition 12 weeks after competitive transplantation, the earliest timepoint in which mutant expansion was observed. We performed ATAC (Assay for Transposase Accessible Chromatin) and CUT&RUN (Cleavage Under Targets & Release Using Nuclease) sequencing in purified CD45.2 HSPCs 12 weeks after competitive transplantation to identify SRCAP and H2A.Z localization. We focused on promoter regions and transcriptional start sites (TSSs) where H2A.Z deposition is associated with repressing transcription.[32–34] Since H2A.Z regulation by SRCAP is not well understood in blood, we first evaluated WT HSPCs to establish the enrichment profile. This revealed 1375 peaks in promoter-TSS regions that were accessible by ATAC and also bound by SRCAP and H2A.Z (Figure 6A and S6A), in agreement with previous findings in other tissues that SRCAP incorporates H2A.Z at promoters.[27,44,45] The corresponding genes of these 1375 peaks were highly enriched in pathways related to histone modification and DNA repair (Figure S6B), correlated with the top differentially expressed pathways in RNA-sequencing result as described above. To further characterize SRCAP-regulated H2A.Z deposition, we performed motif analysis on the SRCAP-enriched peaks and found that the top two were AT-rich binding motifs (Figure 6B), consistent with previous reports showing that SRCAP preferentially binds to AT-rich DNA sequences through its AT hooks in the C-terminus,[27,29] a region that is absent in the SRCAP-Q1963* mutant.

After establishing the characteristics of SRCAP and H2A.Z localization in WT HSPCs, we examined the differential chromatin landscape between *Srcap*$^{mut/+}$ and WT HSPCs with transplantation and doxorubicin treatment. Without stress, *Srcap*$^{mut/+}$ cells showed similar

SRCAP and H2A.Z abundance at the 1375 peak regions (Figure 6C). In WT HSPCs with transplantation and doxorubicin, both SRCAP and H2A.Z were enriched at these regions in response to stress. Importantly, *Srcap*$^{mut/+}$ HSPCs demonstrated a decrease in both SRCAP and H2A.Z localization after exposure to stress (Figure 6C and S6C). Given the corresponding changes in SRCAP and H2A.Z abundance, *Srcap*$^{mut/+}$ cells appear to have decreased SRCAP-regulated H2A.Z deposition under stress compared to WT cells.

With the role of H2A.Z in gene regulation, we examined the relationship between SRCAP-regulated H2A.Z chromatin remodeling and transcriptional regulation by correlating CUT&RUN sequencing with RNA-sequencing results, focusing on the most up-regulated DDR pathway and HSC genes. SRCAP and H2A.Z abundance were both decreased at the promoter regions of these genes after transplantation in the *Srcap*$^{mut/+}$ HSPCs (Figure 6D and S6D), indicating that the transcriptional regulation DDR and HSC genes is dependent on the proper localization of SRCAP and H2A.Z. To assess whether H2A.Z is associated with gene silencing as previously reported,[31–34] we compared RNA-seq expression of genes with H2A.Z localization at the promoters according to CUT&RUN. Indeed, as H2A.Z deposition was decreased in *Srcap*$^{mut/+}$ cells after transplantation, these H2A.Z-bound genes were also transcriptionally upregulated (Figure 6E). This finding indicates that the H2A.Z mark represses gene expression, and that decreased H2A.Z deposition at the promoters of DDR genes is associated with upregulated gene expression. Importantly, decreased H2A.Z deposition was recapitulated in MOLM-13 cells after doxorubicin treatment (Figure S6E).

Interestingly, we assessed a protein-coding gene, Chromobox 8 (*Cbx8*), which is included in the gene set '*positive regulation of DNA repair*' and associated with DNA methylation. *Cbx8* is one of the most highly up-regulated genes and exhibits loss of SRCAP-regulated H2A.Z deposition after transplantation (Figure 6F). We confirmed that H2A.Z is anti-correlated with DNA methylation at this site (Figure S6F). These observations indicate that *Srcap*$^{mut/+}$ stem cells acquire a competitive advantage via epigenetic regulation of the transcriptome.

Together, these data demonstrate that after exposure to transplantation or doxorubicin, *Srcap*$^{mut/+}$ cells lose SRCAP-regulated H2A.Z chromatin remodeling capacity, and the loss correlates with the transcriptional up-regulation of the DDR pathway and of HSC-associated genes (Figure 6G).

Discussion

In this study, we interrogated how *SRCAP* mutations confer a selective advantage leading to clonal hematopoiesis. We showed *SRCAP* mutations are enriched in patients with prior exposure to genotoxic stress and demonstrated *Srcap* lymphoid-biased expansion in a mouse model. We identified doxorubicin and bone marrow transplantation as cellular stressors that promote *Srcap*$^{mut/+}$ expansion via loss of SRCAP-regulated H2A.Z deposition leading to enhanced DNA damage response. We conclude that increased fitness of *Srcap*$^{mut/+}$ stem cells is a result of both altered epigenetic regulation and enhanced DDR, bridging two key pathways that drive CH.

Drug-specific advantage in CH has been previously reported for other mutations such as *PPM1D*.[16] Here, we compared the response to various classes of chemotherapy drugs and showed that *SRCAP*$^{mut/+}$ expansion was promoted by the anthracycline drug doxorubicin more than other agents. This may partially explain the enrichment of *SRCAP* mutations in about 20% (27/154) patients having received chimeric antigen receptor T (CAR-T) cell therapy for lymphoma as they were typically treated with anthracyclines. Because most patients received multi-agent chemotherapy regimens, we could not further assess the selectivity of anthracyclines in patients. Larger human sequencing cohorts with longitudinal analysis will be necessary to assess the contribution of single chemotherapy drugs to CH in patients. Nevertheless, these *in vitro* experiments allow us to dissect specific exposures that contribute to the competitive advantage of *SRCAP*$^{mut/+}$ cells.

Most studies of CH mouse models have reported myeloid-biased differentiation of mutant clones.[46,47] However, we observed a clear lymphoid bias. While lymphoid malignancies are commonly reported in patients with CH,[7] and lymphoid-biased CH is driven by distinct but partially overlapping mutations, they are relatively understudied. Notably, our observation of B-cell expansion accompanied by up-regulated DDR may implicate the role of SRCAP in class switch recombination and related immune functions, which are significantly down-regulated in our RNA-seq data (Figure 5B), potentially impacting immune response by the mutant B cells.[48,49] Consistent with our findings, *SRCAP* mutations are frequently observed in, but not restricted to, patients with lymphoid malignancies.[7,14,25] While we did not observe disease development in the *Srcap* transplanted mice, the 6-month time frame is limited. Interestingly, the phenotype of lymphoid-biased hematopoiesis recapitulates that of *Crebbp* knock-out mice.[50] As the truncation of our *Srcap* mutant model occurs at the end of its CBP-binding domain, it could impair the participation of SRCAP as a co-activator of CBP, leading to reduced CBP activity[51] and consequent lymphoid bias.

We also showed that the selective advantage of *Srcap*$^{mut/+}$ cells could be driven by two distinct cellular stressors: doxorubicin and transplantation, consistent with observations in humans.[14,24] Indeed, both stressors impact epigenetic modifications: anthracyclines rapidly reshape the chromatin landscape and protein-DNA binding,[52,53] and bone marrow transplantation affects DNA methylation,[54] which is negatively associated with H2A.Z mark.[55] Epigenetic reshaping may explain why transplantation and anthracycline treatment most dramatically promote the advantage of *Srcap*$^{mut/+}$ cells relative to other chemotherapy drugs. One of the loci with the most dramatic decrease in SRCAP-regulated H2A.Z deposition, *Cbx8*, is part of the Polycomb complex that also interacts with DNA methyltransferases, implicating DNA methylation in *Srcap* expansion.

Finally, DDR and epigenetics are the two most frequently disrupted pathways in CH, and SRCAP is directly involved in both. *Srcap*$^{mut/+}$ cells acquire increased DDR and survival under stress (similar to cells with *TP53* or *PPM1D* mutations); on the other hand, *Srcap*$^{mut/+}$ stem cells exhibit enhanced HSC function via epigenetic regulation enabling them to outcompete WT clones (similar to *DNMT3A* and *TET2* mutations). Importantly, the increased DDR response in *SRCAP*$^{mut/+}$ cells can be epigenetically regulated. Our work suggests a new perspective that CH mutations may simultaneously and interdependently impact both DDR and epigenetic modifications leading to increased stem cell competition.

Other CH-associated mutations likely impact both pathways, even though they are typically classified into a single group.[22,23]

Limitations of the study

In humans, we observed an enrichment of *SRCAP* mutations in females in cohorts without a known cancer diagnosis. Such female-biased CH has also been associated with additional mutations, particularly the epigenetic modifier *DNMT3A,* as well as the DDR regulator *TP53*.[56] It is possible that chemotherapeutic exposures may also influence the sex bias, but the size of our exposed cohorts limits this analysis. Similarly, *SRCAP* CH has not yet been shown to be associated with adverse clinical outcomes. Larger patient cohorts longitudinally traced with treatment regimens available and detailed long-term clinical follow-up will be necessary to definitively evaluate risks associated with *SRCAP* CH. In addition, the lymphoid bias observed in our murine model is difficult to validate in humans but may be reassessed when larger cohorts of patients are sequenced. Finally, we showed the selection of *SRCAP* mutant cells by anthracycline drug doxorubicin in human cell lines and mice within the time frame of our experimental assay and cannot exclude the possibility of selection by other drugs at a slower rate.

STAR Methods

~~RESOURCE AVAILABILITY~~

Lead contact—Further information and requests for resources should be directed to and will be fulfilled by Lead Contact, Margaret A. Goodell (goodell@bcm.edu).

Materials availability—This study generated heterozygous *SRCAP*-mutant cell lines and *Srcap*-mutant mice. The human cell lines and mouse line generated by the Goodell laboratory are available upon request and will require a standard Material Transfer Agreement (MTA).

Data and code availability

- All raw and processed sequencing data generated in this work is publicly available at GEO data repository as of the date of publication. Accession number is listed as key resources table. Microscopy data reported in this paper will be shared by the lead contact upon request.
- No original code for analysis in this work.
- Any additional information required to reanalyze the data reported in this paper is available from the lead contact upon request.

~~EXPERIMENTAL MODEL AND STUDY PARTICIPANT DETAILSs~~

Cell Culture and CRISPR/Cas9 genetic engineering: MOLM-13 cells were cultured in RPMI 1640 medium supplemented with 10% FBS, 1% penicillin/streptomycin/glutamine, U-2 OS cells and HEK293T cells were cultured in DMEM supplemented with 10% FBS and 1% Pen/Strep. All cells were cultured in humidified incubator containing 5% CO_2 at 37°C.

MOLM-13 cells were grown in T-25 flasks and passaged approximately every three days. U-2 OS cells and HEK293T cells were grown in 10 cm^2 dishes and passaged every three to four days with trypsin. All experiments involving isolation of single colonies were compared between mutant and isogenic control lines from the same parental line. The sex of the cell lines is as follows: HEK293T (female), MOLM-13 (male), U-2 OS (female).

We generated the heterozygous *SRCAP* mutant (*SRCAP*$^{mut/+}$) cell lines in MOLM-13 and U-2 OS as well as GFP-positive MOLM-13 cell line using RNP-based CRISPR/Cas9 delivery method as described in Huang et al., 2022[10]. In brief, 1 μg sgRNA (Synthego) was incubated with 1 μg Cas9 protein (PNA Bio) for 30 minutes at room temperature to obtain Cas9-sgRNA RNPs. Next, 1.2 μg single-stranded DNA donor template (Integrated DNA Technologies) (see Table S2 for guide RNA and donor DNA sequences) containing desired variant sequence was added prior to electroporation using a Neon transfection system (Thermo Fisher Scientific), and 2×10^5 cells were electroporated using the optimized electroporation condition of 1,350 V, 35 ms, and one pulse for MOLM-13, or 1,230 V, 10 ms, and four pulse for U-2 OS. After electroporation, we collected single-cell colonies for each cell line, and the sequences of single colonies were validated by Sanger sequencing.

Mice Housing and generation of *Srcap*-mutant murine model: All mice were housed in AAALAC-accredited, specific-pathogen-free animal care facilities at Baylor College of Medicine, and all procedures were approved by the BCM Institutional Animal Care and Use Committee. Mice of both sexes were used for all experiments. All mice were immune-competent and healthy prior to the experiments described.

We generated the heterozygous *Srcap* mutant (*Srcap*$^{mut/+}$) knock-in murine model using CRISPR/Cas9 technology in collaboration with the Mouse Embryonic Stem Cell Core and Genetically Engineered Rodent Models Core at Baylor College of Medicine. A sgRNA was designed to induce a double-stranded break in the endogenous *Srcap* exon 26 along with a single-stranded oligodeoxynucleotide (ssODN) containing a 3x FLAG tag followed by a premature stop codon flanked by proximal and distal homology arms for homology-directed repair (see Table S2 for guide RNA and donor DNA sequences). A total of 200 C57BL/6 embryos were injected to the cytoplasm with 100 ng/μL Cas9 protein, 20 ng/μL sgRNA, and 100 ng/μL ssODN diluted in nuclease-free PBS. After culture, about 20 to 30 blastocysts were transferred into the oviducts of pseudo-pregnant ICR females. Genotype identification of *Srcap*$^{mut/+}$ mice was performed with genotyping primers and Sanger Sequencing (see Table S2), then CRISPR on-target and top ten predicted off-target sites were screened using PCR (see Table S2). *Srcap*$^{mut/+}$ mice showed normal breeding and appearance. Germline *Srcap*$^{mut/+}$ mice exhibited no altered hematopoiesis in hematopoietic stem cell properties or downstream lineage distribution. We used the progeny following at least F4 for experiments in this work.

~~METHOD DETAILS~~

SRCAP analysis in the UK Biobank and MGB Biobank cohort: Somatic variations in the *SRCAP* gene region were queried in the whole-exome sequencing data from 180,465 unrelated participants (99,184 female and 81,281 male) with no prior hematologic

malignancies in the UK Biobank.[68] Somatic mutations in the whole exome sequencing (WES) data from each participant were called using Mutect2.[69] The Genome Aggregation Database[70] (gnomAD) used a germline reference and a panel-of-normal consisting of randomly selected 500 youngest participants were used to filter out artifacts. The mutations were included if all of the following criteria were met:

1. Sequencing depth (DP) >= 20
2. Reads supporting the variant allele (AD) >= 3
3. Reads supporting in both forward and reverse direction (F1R2 & F2R1) >= 1
4. Variant allele fraction (VAF) >= 0.02 & < 0.35
5. gnomAD allele frequency < 0.005
6. variant frequency in the cohort < 0.01
7. AD for insertions and deletion in homopolymer regions >= 10 and VAF >= 0.1

In total, we identified 141 participants with at least one pathogenic somatic mutation in the SRCAP gene. Only frameshift, nonsense, and splice site variants were considered pathogenic.

SRCAP analysis in CAR-T and melanoma cohorts: Somatic variant calling was done as described previously.[39] Mutations with five or more alternative reads were considered in analysis. Mutations with a variant allele fraction (VAF) greater than 0.35 were excluded to avoid inclusion of germline variants.

Mouse genotyping: Mouse DNA was extracted from mouse tails using DirectPCR Lysis Buffer (Viagen, 102-T) with 0.3 mg/ml Proteinase K (genDEPOT, P2180). Forward and reverse primer pairs were designed targeting *Srcap* exon 26 in *Srcap*$^{mut/+}$ mice (see Table S2). The PCR product was 291 bp for the WT allele and 375 bp for the mutant allele containing a 3x FLAG tag and a premature stop codon.

DNA constructs and cloning: Human SRCAP ORF Clone in Gateway Cloning Vector (Antibodies-online, ABIN3417640) was used to acquire the SRCAP overexpression plasmid. SRCAP WT and truncated mutant proteins were each tagged with an in-frame *C*-terminal 3x FLAG tag. SRCAP ORF template sequence was amplified with PCR. For WT SRCAP, two PCR amplifications were performed separately to acquire the first and second half of SRCAP (~4.8 kb each) and assemble them into full-length SRCAP (~9.7 kb). For mutant SRCAP, a similar strategy was adopted to amplify two PCR products before constructing into truncated SRCAP (~5.9 kb). The vector backbone with Ampicillin resistance gene was acquired from VectorBuilder and amplified. All the PCR products were purified using QIAquick Gel Extraction Kit (Qiagen, 28704) and validated using Sanger Sequencing. Plasmids were then generated with 4-fragment Gibson Assembly using NEBuilder® HiFi DNA Assembly Master Mix (New England BioLabs, E2621S). The assembled products were then transformed into TOP10 competent cells and selected on LB plates with Ampicillin (50 μg/ml) overnight before plasmid extraction and validation with Sanger Sequencing.

Real-time quantitative reverse transcription PCR: RNA was extracted from AllPrep DNA/RNA micro kit (Qiagen, 80284) from cells. 1 μg of RNA was mixed with 4 μL iScript™ Reverse Transcription Supermix (Bio-rad, 1708841) and 15 μL nuclease-free water. The mixture was incubated in the thermocycler for 5 minutes at 25 °C for priming, followed by 20 minutes at 46 °C for reverse transcription and 1 minutes at 95 °C for inactivation. The reverse transcription cDNA product was diluted 10-fold. 1 μL diluted cDNA was then mixed with 1 μL of 10 μmol/L forward and reverse primers (see Table S2), 8 μL ddH2O, and 10 μL 2× SsoAdvanced Universal SYBR Green Supermix (Bio-rad, 1725271) for real-time PCR. Samples were heat activated at 95°C for 3 minutes, then kept at 95°C for 10 seconds, 58°C for 10 seconds, and 72°C for 30 seconds and repeated from the second step for 40 cycles. The cycle threshold (Ct) values of reactions were determined for analysis.

Cytotoxic drug-sensitivity assay: Drug sensitivity assays were done using the Cell Proliferation MTT Kit (Sigma, 11465007001) per manufacturer's protocol. Briefly, 1×10^4 cells were plated in 96-well, flat bottom plates and treated with vehicle or drugs in a total volume of 100 uL. Plates were incubated at 37°C for at least 24 hours. 10 uL of MTT labeling reagent was added to each well and incubated for 4 hours. 100 uL of solubilization buffer was then added to each well and incubated overnight. Plates were analyzed using a fluorometric microplate reader at 550 nm.

Apoptosis assay: FITC Annexin V Apoptosis Detection Kit I (BD Bioscience, 556547) was used for the quantification of early and late apoptotic cells. Cells were treated with each drug for 48 hours. Cells are treated to IC50 of the drug to assess apoptotic response. After drug treatment, cells were washed and stained with annexin V-FITC (3:100 concentration) and 7-AAD (3:100 concentration) for 20 minutes. Cells were then analyzed using flow cytometry (LSRII, Becton Dickinson) with FACSdiva software (BD Bioscience). A minimum of 10,000 cells were analyzed per sample.

***In vitro* cell cycle assay:** FITC BrdU Flow Kit (BD Bioscience, 559619) was used for cell cycle assay with MOLM-13 cell line according to the manufacturer's protocol. Cells are treated to IC60 of the drug to minimize the impact of apoptosis and assess the difference in cell cycle distribution. In brief, cells were treated with cytotoxic drugs for 24 hours and then paused with 50 μM BrdU in the media for 40 minutes before harvesting. The BrdU-pulsed cells were fixed and permeabilized. The cells were then re-fixed, treated with 100 μL DNase (300 μg/mL) at 37°C for 1 hour, and stained with intracellular FITC-BrdU antibody at room temperature for 20 minutes. DNA staining with 20 μL 7-AAD was performed before flow cytometry analysis (LSRII, Becton Dickinson) with FACSdiva software (BD Bioscience). A minimum of 20,000 cells were analyzed per sample.

***In vivo* cell cycle assay:** FITC BrdU Flow Kit (BD Bioscience, 559619) was used for murine bone marrow according to the manufacturer's protocol. In brief, mice were intraperitoneally injected with 200 μL BrdU solution (10 mg/mL) in sterile PBS. Whole bone marrow was harvested and enriched for HSC 24 hours post-injection. The enriched bone marrow cells were stained with surface markers, fixed and permeabilized. The cells were then re-fixed, treated with 100 μL DNase (300 μg/mL) at 37°C for 1 hour, and stained

with intracellular FITC-BrdU antibody at room temperature for 20 minutes. DNA staining with 20 μL 7-AAD was performed before analyzing using flow cytometry (LSRII, Becton Dickinson) with FACSdiva software (BD Bioscience). A minimum of 10,000,000 cells were analyzed per sample to assess HSC cell cycle.

Cell-based competition Assay: In the cell-based competition assay, *GFP* is knocked in endogenously in-frame at the *AAVS1* safe harbor locus. Isogenic mutant GFP-negative MOLM-13 cells were mixed with WT GFP-positive cells at a 10% to 90% ratio in 6 well plates with a total of 2×10^5 cells per well. The cell mixtures were treated with cytotoxic drugs or DMSO as control. Cells are treated to IC75 of the drug to evaluate the impact to apoptosis and cell cycle gradually over time. The mixture was assayed with flow cytometry to monitor the percentage of GFP-negative and GFP-positive portion every two days after treatment. At each timepoint, cells were spun down and replenished with fresh 5 mL cell culture medium with appropriate concentration of drugs.

Alkaline comet assay: Comet assays were conducted with mouse bone marrow cells by resuspending to 1×10^5 cells/mL and mixed with 1% low-melting agarose (R&D Systems, 4250–050-02) at a 1:10 ratio and plated on 2-well CometSlides (R&D Systems, 4250–050-03). Cells were lysed overnight and immersed in alkaline unwinding solution as per manufacturer's protocol (Trevigen, 4250–050-ESK). Fluorescence microscopy was performed at 10X magnification using the Keyence BZ-X800 microscope and comet tails were analyzed using the Comet Assay IV software (Instem). At least 150 comet tails were measured per sample.

GFP-based DNA repair (HR or NHEJ) reporter assay: For the DNA repair reporter assay, 100,000 U-2 OS cells were seeded in a 12-well plate. After attachment to the plate, cells were transfected with 3.6 uL of Lipofectamine 2000 (Invitrogen) in 200 uL of OptiMEM with 0.8 ug of the I-SceI expression plasmid (pCBASce). The media was replaced after 12 hours, and the cells were trypsinized 48 hours after transfection for flow cytometry analysis GFP-positive population and proportion.

Immunoblotting: Protein lysates were harvested with Cytobuster (Millipore, 71009–3) buffer supplemented with protease inhibitor cocktail for 15 min at 4°C and then boiled at 95°C in 1x Laemmli sample buffer (Bio-rad, 1610747) for 7 minutes. The proteins were separated by 4–15% mini-PROTEAN TGX precast protein gels (Bio-rad, 456–1084) and transferred on to PVDF membranes using the iBlot 2 Dry Blotting system (ThermoFisher, IB21001). Blots were blocked 5% milk in Tris-buffered saline solution with 0.05% Tween-20 (TBST) for 1 hour at room temperature. After washing with TBST, blots were then probed with different primary antibodies overnight at 4°C. Blots were washed with TBST before incubation with secondary antibodies conjugated with Horseradish Peroxidase (HRP) for 45 minutes at room temperature. After washing with TBST, imagines were taken using Clarity ECL Substrate on the ChemiDoc imaging system (Bio-rad).

Immunofluorescence: Before staining, 3×10^5 cells/slide were harvested and washed with PBS three times. The cells were then fixed with 4% paraformaldehyde for 10 minutes at 37°C and washed with PBS three times. Fixed cells were resuspended in PBS and

cytocentrifuge was performed at 250 rpm for 4 min to attach the cells to the slide. The cells on the slide were then permeabilized with 0.5% Triton-X-100 in PBS at room temperature for 20 minutes, washed with PBS, and blocked with 1% BSA in 15% goat serum at room temperature 1 hour. Samples were then stained with different primary antibodies in 0.1% BSA in PBS at 4°C overnight. The following day, samples were washed with 0.01% Triton-X-100 in PBS before staining with secondary antibodies conjugated with fluorophores at room temperature for 1 hour. Samples were washed with 0.01% Triton-X-100 in PBS and then mounted onto slides with Fluoromount-G Mounting Medium with DAPI (ThermoFisher, 00–4959-52) and sealed with nail polish. Immunostained coverslips were imaged on the Keyence BZ-X800 microscope.

Flow cytometry intracellular staining: Murine bone marrow cells for intercellular staining were harvested, fixed and permeabilized using BD Cytofix/Cytoperm Buffer. The fixed cells were then stained with FITC-γH2A.X antibody at 4°C for 20 minutes. Fluorescence intensity was analyzed using flow cytometry (LSRII, Becton Dickinson) with FACSdiva software (BD Bioscience). A minimum of 10,000,000 cells were analyze per sample.

Colony formation Assay: Fresh bone marrow cells harvested from mice were seeded in 6 well plates at a density of 250 cell/well in 3 mL Methocult (STEMCELL Technology, M3434) for 7 days. Number of colonies were quantified at Day7 for primary plating using a microscope. The cells were then collected from each well, washed with phosphate-buffered saline (PBS), resuspended with fresh 3 mL of Methocult, and seeded again in 6 well plates for 7 days. At Day 14, the number of colonies was quantified for secondary plating.

Murine competitive bone marrow transplantation: We utilized the CD45 allelic system to perform murine competitive bone marrow transplantation. Bone marrow from WT or mutant donor mice (bearing the CD45.2 surface alloantigen) was harvested and combined with bone marrow from WT recipient mice (bearing the CD45.1 surface alloantigen). Cell numbers for each sample were quantified, and test cells (CD45.2) were mixed with competitor cells (CD45.1) at a 10:90 ratio, resulting in a mutant (CD45.2) with WT (CD45.1) mixture and a WT (CD45.2) with WT (CD45.1) mixture as parallel control. We calculated a total of 2×10^6 cells to transplant into each recipient mouse, consisting of 0.2×10^6 test Cd45.2 cells and 1.8×10^6 CD45.1 cells. Next, the bone marrow mixtures were retro-orbitally injected into 6- to 8-week-old lethally irradiated recipient mice (split-dose of 10 Gy separated by 3 hours) in both the mutant and parallel control cohort.

The recipient mice were bled every 4 weeks post-transplantation for donor (CD45.2) cell chimerism and lineage composition analyses in the peripheral blood with flow cytometry (BD Biosciences, LSR II for data acquisition and FlowJo software for analysis). All data points were normalized to the data at the 4-weeks timepoint in each mouse as baseline engraftment. After 20 weeks post-transplantation, the recipient mice were bled and sacrificed to harvest peripheral blood, bone marrow, spleen, and thymus for further enrichment and analysis.

Hematopoietic stem cell enrichment: Bone marrow from the mice were harvested with HBSS (2% FBS, 5% HEPES, and 40 μM EDTA) and the whole bone marrow underwent lysis of red blood cells. Cells were then incubated with CD117-conjugated Microbeads (Miltenyi, 130–091-224) at 4 °C for 30 minutes. Unbound beads were removed by washing with PBS. Then, the mixture was applied to the QuadroMacs column (Miltenyi, 130–042-401), followed by two washes with 5 mL HBSS. CD117-enriched bone marrow cells were eluted with 5 mL HBSS using a plunger.

RNA-sequencing: Cells were sorted directly into Lysis Buffer, and RNA was isolated using the Allprep DNA/RNA Micro Kit (Qiagen). RNA-sequencing was performed with True-Seq Stranded mRNA library preparation kit (Illumina, 20020594) according to the manufacturer's protocol. Quality control of libraries was performed using a TapeStation D1000 ScreenTape (Agilent, 5067–5584). Libraries were then sequenced using an Illumina Nextseq 2000 sequencer, aiming for >20 million reads per biological replicate. Paired-end RNA-sequencing reads were obtained.

Single-cell RNA-sequencing: Single-cell RNA-sequencing was performed with isolated hematopoietic stem and progenitor cells (HSPCs) from the bone marrow using the 10x platform 3v31 assay and the chromium Single Cell 3' solution without multiplexing. Quality control of libraries was done with TapeStation D1000 ScreenTape (Agilent, 5067–5584). Libraries were then sequenced using an Illumina Nextseq 2000 sequencer, aiming for a minimum coverage of 30,000 reads per single cell. Paired-end (read1: 28 cycles; i7 index: 10 cycles; i5 index: 10 cycles; read2: 90 cycles) single-cell RNA-sequencing reads were obtained.

ATAC-sequencing: ATAC-sequencing for chromatin accessibility was performed using the Omni-ATAC protocol. In brief, 20,000 mouse bone marrow cells were isolated, washed, and permeabilized with ATAC-Resuspension Buffer (10 mM Tris-HCl, pH7.4, 10 mM NaCl, 3 mM $MgCl_2$ in sterile water) containing 0.1% NP40, 0.1% Tween-20, and 0.01% Digitonin for 3 minutes on ice. The lysis was washed, and nuclei were pelleted for transposition in 50 μL Transposition mix (25 μL 2x TD buffer, 2.5 μL Tn5 transposases, 16.5 μL PBS, 0.5 μL 1% digitonin, 0.5 μL 10% Tween-20, 5 μL ddH_2O) with enzymes from Nextera XT DNA Library Preparation Kit (Illumina, FC-131–1096). The mixture was then incubated at 37 °C for 30 minutes and cleaned up with DNA Clean & Concentrator (Zymo, D4030).

ATAC-sequencing library preparation was performed using NEBNext® Ultra™ II DNA Library Prep Kit for Illumina (New England Biolabs, E7645) according to the manufacturer's protocol. Quality control of libraries was done with TapeStation D5000 ScreenTape (Agilent, 5067–5588). Libraries were then sequenced using Illumina Nextseq 2000 sequencer, aiming for >50 million reads per biological replicate. Paired-end DNA-sequencing reads were obtained.

Cut-and-run sequencing: Cut-and-run sequencing was performed using Epicypher® CUTANA™ CUT&RUN protocol (V2.0). In brief, 50,000 cells were harvested or sorted, and washed with Wash Buffer (20 mM HEPES, pH 7.5, 150 mM NaCl, 0.5 mM Spermidine, 1x Roche cOmplete™, Mini, EDTA-free Protease Inhibitor tab) at room temperature three

times. The cells were then incubated with ConA beads (Promega, BP531) activated with iced Bead Activation Buffer (20 mM HEPES, pH7.9, 10 mM KCl, 1 mM $CaCl_2$, 1 mM $MnCl_2$) at room temperature for 20 minutes on a rotator. After the incubation, the cells conjugated with beads were transferred to 8-strip tubes for binding with primary antibody (1:100) in 100 μL Antibody Buffer (Wash Buffer, 0.01% Digitonin, 2 mM EDTA) on a nutator overnight at 4°C. The next day, the beads were washed three times with Digitonin Buffer (Wash Buffer, 0.01% Digitonin) and incubated with pAG-MNase (1:20) in Digitonin Buffer on nutator for 20 minutes at room temperature. Targeted chromatin cleavage was performed after three washes with 100 mM $CaCl_2$ in Digitonin Buffer on nutator for 2 hours at 4°C. Targeted DNA was released with 33 μL Stop Buffer (340 mM NaCl, 20 mM EDTA, 4 mM EGTA, 50 μg/mL RNase A, 50 μg/mL Glycogen) and incubated for 10 minutes at 37°C. Finally, DNA released in the supernatant was collected and purified with CUTANA™ DNA Purification Kit (Epicypher, 14–0050) according to the manufacturer's protocol.

Cut-and-run sequencing library preparation was performed using NEBNext® Ultra™ II DNA Library Prep Kit for Illumina (New England Biolabs, E7645) according to the manufacturer's protocol. Quality control of libraries was done with TapeStation D5000 ScreenTape (Agilent, 5067–5588). Libraries were then sequenced using Illumina Nextseq 2000 sequencer, aiming for >10 million reads per condition. Paired-end enriched DNA-sequencing reads were obtained.

~~QUNATIFICATION AND STATISTICAL ANALYSIS~~

Immunofluorescence foci analysis: High resolution imaging was obtained on a Cytivia DVLive epifluorescence image restoration microscope with an Olympus PlanApo 60×/1.42 NA objective. Z stacks (0.25 μm) were acquired before applying a conservative restorative algorithm for quantitative image deconvolution. Random fields of view (FOVs) were acquired for analysis. Then, automated image analysis was performed using CellProfiler v.4.2.1 with the following pipeline: first, the DAPI channel was smoothed (median filter) and then used to identify nuclei with minimum cross entropy algorithm and filtered by size (40–120 pixels); second, the γH2Ax signal was thresholded using otsu to identify individual spots ("foci") from the antibody channel; next, the identified foci where then related to the parent nuclei; finally, foci counts and intensity features were extracted for post-analysis.

RNA-sequencing analysis: Paired-end bulk RNA-sequencing reads were mapped to the STAR mouse reference genome index (mm39) using STAR. Quantification of mapped reads for RNA-sequencing was performed using Subread package (featureCounts). Read count normalization of all conditions and differential analysis were then performed using DESeq2 package. At least two biological replicates were used for differential analysis, and genes with average read counts <15 per sample were excluded for differential analysis for each condition (WT pre-treatment to WT post-treatment, mutant pre-treatment to mutant post-treatment, or WT post-treatment to mutant post-treatment). DESeq2 utilizes the degree of freedom equals to two for duplicates to estimate dispersion and calculate differential expression with statistical significance. The fold change and statistical outputs for each

comparison were used for downstream Gene Set Enrichment Analysis (GSEA), gene list subsetting, and figure plotting.

Single-cell RNA-sequencing analysis: Paired-end sequencing data were mapped and quantified using Cell Ranger Single Cell Suite v3.1.0 to the mouse genome (mm10) provided by 10x Genomics' Cell Ranger. Cells with 6,500–30,000 detected genes and less than 10% total mitochondrial gene expression were filtered and retained for analysis. R package scuttle was used to normalize for library size and perform log-transformation. Next, R package scran was used to perform feature selection of highly variable genes for dimensional reduction via principal component analysis (PCA). The resulting principal components were visualized using Uniform manifold approximation and projection (UMAP) and used to cluster the cells. Clusters were identified by fitting the top 13 principal components as determined by PCA elbow method to compute a neighborhood graph with the center of 15 using R scran package. Cells were then clustered into subgroups using SingleR package referencing mouse Immunologic Genome Project (ImmGen) data obtained from R celldex package. Differential analysis of each cell type clusters was performed using edgeR. The fold change and statistical outputs for each comparison were used for downstream Gene Set Enrichment Analysis (GSEA), gene list subsetting, and figure plotting.

ATAC-sequencing analysis: Paired-end sequencing data were mapped to the mouse genome (mm10) using Bowtie2 with command line option "--dovetail". ATAC peaks were shifted using deepTools alignmentSieve with command line option "--ATACshift". Biological replicates were then merged for peak calling using MACS3 with command line options "-g mm -f BAMPE -q 0.01 --nomodel --keep-dup=all --call-summits". HOMER was used to annotate peaks in the TF peak regions identified by MACS3. Quantification of peaks for ATAC-sequencing was performed using Subread package. The count results were used for differential analysis and statistics with DESeq2 package. At least two biological replicates were used for differential analysis, and genes with average read counts <100 per sample were excluded for differential analysis for each condition. Peak region identified by MACS3 with the 3kb region centered around the transcriptional start site were used for candidate gene RefSeq annotations and figure plotting.

Cut-and-run sequencing analysis: Paired-end sequencing data were mapped to the mouse genome (mm10) using Bowtie2 with command line option "--dovetail". Cut-and-run reads from biological replicates were then merged for peak calling using MACS3 with command line options "-g mm -f BAMPE -q 0.01 --nomodel --keep-dup=all --call-summits". HOMER was used to annotate peaks in the TF peak regions identified by MACS3. Quantification of peaks for Cut-and-run sequencing was performed using Subread package. The count results were used for differential analysis and statistics with DESeq2 package. At least two biological replicates were used for differential analysis, and genes with average read counts <50 per sample were excluded for differential analysis for each condition. Peak region identified by MACS3 with the 3kb region centered around the transcriptional start site were used for candidate gene RefSeq annotations and figure plotting. Top binding motifs were discovered and characterized using R memes package.

Statistical analysis: Statistical tests were applied with the sample size listed in the Figure Legends. Sample size represents the number of independent biological replicates (denoted by "n"). Data supporting the main conclusions represents results from at least two biological replicates. Graphs with error bars report mean ± SEM or mean ± SD as indicated in the Figure Legends. Statistics were calculated using two-tailed *t*-tests, without assuming equal standard deviations, unless otherwise indicated. PRISM was used for basic statistical analysis and figure generation (https://www.graphpad.com), and the R language and programming environment (https://www.r-project.org) was used for the remainder of statistical analysis. Multiple hypothesis testing correction was applied where indicated. Statistical significance was determined using GraphPad PRISM and indicated in the figures. Data were considered statistically significant at *p<0.05, **p<0.01, ***p<0.001.

Supplementary Material

Refer to Web version on PubMed Central for supplementary material.

Acknowledgements

This project was supported by the Cytometry and Cell Sorting Core (CPRIT-RP180672 and CA125123) and Genetically Engineered Rodent Models Core at Baylor College of Medicine. This work was supported by AG036695, CA237291, 1P01CA265748, DK092883. AS was supported by K08CA252174 and DOD CA210827. AN was supported by funds from the Knut and Alice Wallenberg Foundation (no. KAW2017.0436). PGM was supported by K08CA263183 and the Edward P. Evans Foundation. Work in EpiCypher was supported by R44 (HG011875, CA212733, GM136172, CA212733 and DE029633). PN was supported by NHLBI R01HL148050, NHLBI R01HL148565, Foundation Leducq TNE-18CVD04.

Competing Interests

AS: consulting fees from Novartis and Roche. P.N: research grants from Allelica, Apple, Amgen, Boston Scientific, Genentech / Roche, and Novartis, personal fees from Allelica, Apple, AstraZeneca, Blackstone Life Sciences, Foresite Labs, Genentech / Roche, GV, HeartFlow, Magnet Biomedicine, and Novartis, scientific advisory board membership of Esperion Therapeutics, Preciseli, and TenSixteen Bio, scientific co-founder of TenSixteen Bio, equity in Preciseli and TenSixteen Bio, and spousal employment at Vertex Pharmaceuticals, all unrelated to the present work. EpiCypher is a commercial developer and supplier of reagents and platforms used in this study. SP are employed by (and own shares in) New England Biolabs. BJV and MCK are employed by (and own shares in) EpiCypher. MCK is a board member of EpiCypher.

Inclusion and Diversity

We support inclusive, diverse, and equitable conduct of research.

References:

1. Cagan A, Baez-Ortega A, Brzozowska N, Abascal F, Coorens THH, Sanders MA, Lawson ARJ, Harvey LMR, Bhosle S, Jones D, et al. (2022). Somatic mutation rates scale with lifespan across mammals. Nature 604, 517–524. 10.1038/s41586-022-04618-z. [PubMed: 35418684]
2. Martincorena I (2019). Somatic mutation and clonal expansions in human tissues. Genome Med 11, 35. 10.1186/s13073-019-0648-4. [PubMed: 31138277]
3. Mitchell E, Spencer Chapman M, Williams N, Dawson KJ, Mende N, Calderbank EF, Jung H, Mitchell T, Coorens THH, Spencer DH, et al. (2022). Clonal dynamics of haematopoiesis across the human lifespan. Nature 606, 343–350. 10.1038/s41586-022-04786-y. [PubMed: 35650442]
4. Jaiswal S, and Ebert BL (2019). Clonal hematopoiesis in human aging and disease. Science 366. 10.1126/science.aan4673.

5. Young AL, Challen GA, Birmann BM, and Druley TE (2016). Clonal haematopoiesis harbouring AML-associated mutations is ubiquitous in healthy adults. Nat Commun 7, 12484. 10.1038/ncomms12484. [PubMed: 27546487]
6. Arends CM, Galan-Sousa J, Hoyer K, Chan W, Jager M, Yoshida K, Seemann R, Noerenberg D, Waldhueter N, Fleischer-Notter H, et al. (2018). Hematopoietic lineage distribution and evolutionary dynamics of clonal hematopoiesis. Leukemia 32, 1908–1919. 10.1038/s41375-018-0047-7. [PubMed: 29491455]
7. Niroula A, Sekar A, Murakami MA, Trinder M, Agrawal M, Wong WJ, Bick AG, Uddin MM, Gibson CJ, Griffin GK, et al. (2021). Distinction of lymphoid and myeloid clonal hematopoiesis. Nat Med 27, 1921–1927. 10.1038/s41591-021-01521-4. [PubMed: 34663986]
8. Challen GA, and Goodell MA (2020). Clonal hematopoiesis: mechanisms driving dominance of stem cell clones. Blood 136, 1590–1598. 10.1182/blood.2020006510. [PubMed: 32746453]
9. Watson CJ, Papula AL, Poon GYP, Wong WH, Young AL, Druley TE, Fisher DS, and Blundell JR (2020). The evolutionary dynamics and fitness landscape of clonal hematopoiesis. Science 367, 1449–1454. 10.1126/science.aay9333. [PubMed: 32217721]
10. Huang YH, Chen CW, Sundaramurthy V, Slabicki M, Hao D, Watson CJ, Tovy A, Reyes JM, Dakhova O, Crovetti BR, et al. (2022). Systematic Profiling of DNMT3A Variants Reveals Protein Instability Mediated by the DCAF8 E3 Ubiquitin Ligase Adaptor. Cancer Discov 12, 220–235. 10.1158/2159-8290.CD-21-0560. [PubMed: 34429321]
11. Zhang X, Su J, Jeong M, Ko M, Huang Y, Park HJ, Guzman A, Lei Y, Huang YH, Rao A, et al. (2016). DNMT3A and TET2 compete and cooperate to repress lineage-specific transcription factors in hematopoietic stem cells. Nat Genet 48, 1014–1023. 10.1038/ng.3610. [PubMed: 27428748]
12. Bolton KL, Ptashkin RN, Gao T, Braunstein L, Devlin SM, Kelly D, Patel M, Berthon A, Syed A, Yabe M, et al. (2020). Cancer therapy shapes the fitness landscape of clonal hematopoiesis. Nat Genet 52, 1219–1226. 10.1038/s41588-020-00710-0. [PubMed: 33106634]
13. Coombs CC, Zehir A, Devlin SM, Kishtagari A, Syed A, Jonsson P, Hyman DM, Solit DB, Robson ME, Baselga J, et al. (2017). Therapy-Related Clonal Hematopoiesis in Patients with Non-hematologic Cancers Is Common and Associated with Adverse Clinical Outcomes. Cell Stem Cell 21, 374–382 e374. 10.1016/j.stem.2017.07.010. [PubMed: 28803919]
14. Wong TN, Miller CA, Jotte MRM, Bagegni N, Baty JD, Schmidt AP, Cashen AF, Duncavage EJ, Helton NM, Fiala M, et al. (2018). Cellular stressors contribute to the expansion of hematopoietic clones of varying leukemic potential. Nat Commun 9, 455. 10.1038/s41467-018-02858-0. [PubMed: 29386642]
15. Miller PG, Sperling AS, Brea EJ, Leick MB, Fell GG, Jan M, Gohil SH, Tai YT, Munshi NC, Wu CJ, et al. (2021). Clonal hematopoiesis in patients receiving chimeric antigen receptor T-cell therapy. Blood Adv 5, 2982–2986. 10.1182/bloodadvances.2021004554. [PubMed: 34342642]
16. Hsu JI, Dayaram T, Tovy A, De Braekeleer E, Jeong M, Wang F, Zhang J, Heffernan TP, Gera S, Kovacs JJ, et al. (2018). PPM1D Mutations Drive Clonal Hematopoiesis in Response to Cytotoxic Chemotherapy. Cell Stem Cell 23, 700–713 e706. 10.1016/j.stem.2018.10.004. [PubMed: 30388424]
17. Kahn JD, Miller PG, Silver AJ, Sellar RS, Bhatt S, Gibson C, McConkey M, Adams D, Mar B, Mertins P, et al. (2018). PPM1D-truncating mutations confer resistance to chemotherapy and sensitivity to PPM1D inhibition in hematopoietic cells. Blood 132, 1095–1105. 10.1182/blood-2018-05-850339. [PubMed: 29954749]
18. Gibson CJ, Lindsley RC, Tchekmedyian V, Mar BG, Shi J, Jaiswal S, Bosworth A, Francisco L, He J, Bansal A, et al. (2017). Clonal Hematopoiesis Associated With Adverse Outcomes After Autologous Stem-Cell Transplantation for Lymphoma. J Clin Oncol 35, 1598–1605. 10.1200/JCO.2016.71.6712. [PubMed: 28068180]
19. Challen GA, Sun D, Jeong M, Luo M, Jelinek J, Berg JS, Bock C, Vasanthakumar A, Gu H, Xi Y, et al. (2011). Dnmt3a is essential for hematopoietic stem cell differentiation. Nat Genet 44, 23–31. 10.1038/ng.1009. [PubMed: 22138693]
20. Gu T, Lin X, Cullen SM, Luo M, Jeong M, Estecio M, Shen J, Hardikar S, Sun D, Su J, et al. (2018). DNMT3A and TET1 cooperate to regulate promoter epigenetic landscapes in mouse embryonic stem cells. Genome Biol 19, 88. 10.1186/s13059-018-1464-7. [PubMed: 30001199]

21. Yang L, Rodriguez B, Mayle A, Park HJ, Lin X, Luo M, Jeong M, Curry CV, Kim SB, Ruau D, et al. (2016). DNMT3A Loss Drives Enhancer Hypomethylation in FLT3-ITD-Associated Leukemias. Cancer Cell 30, 363–365. 10.1016/j.ccell.2016.07.015.
22. Maifrede S, Le BV, Nieborowska-Skorska M, Golovine K, Sullivan-Reed K, Dunuwille WMB, Nacson J, Hulse M, Keith K, Madzo J, et al. (2021). TET2 and DNMT3A Mutations Exert Divergent Effects on DNA Repair and Sensitivity of Leukemia Cells to PARP Inhibitors. Cancer Res 81, 5089–5101. 10.1158/0008-5472.CAN-20-3761. [PubMed: 34215619]
23. Chen S, Wang Q, Yu H, Capitano ML, Vemula S, Nabinger SC, Gao R, Yao C, Kobayashi M, Geng Z, et al. (2019). Mutant p53 drives clonal hematopoiesis through modulating epigenetic pathway. Nat Commun 10, 5649. 10.1038/s41467-019-13542-2. [PubMed: 31827082]
24. Slavin TP, Teh JB, Weitzel JN, Peng K, Wong FL, Qin H, Wang J, Wu X, Mei M, Pillai R, et al. (2019). Association between Clonal Hematopoiesis and Late Nonrelapse Mortality after Autologous Hematopoietic Cell Transplantation. Biol Blood Marrow Transplant 25, 2517–2521. 10.1016/j.bbmt.2019.08.013. [PubMed: 31445185]
25. Beauchamp EM, Leventhal M, Bernard E, Hoppe ER, Todisco G, Creignou M, Galli A, Castellano CA, McConkey M, Tarun A, et al. (2021). ZBTB33 is mutated in clonal hematopoiesis and myelodysplastic syndromes and impacts RNA splicing. Blood Cancer Discov 2, 500–517. 10.1158/2643-3230.BCD-20-0224.
26. Feng Y, Tian Y, Wu Z, and Xu Y (2018). Cryo-EM structure of human SRCAP complex. Cell Res 28, 1121–1123. 10.1038/s41422-018-0102-y. [PubMed: 30337683]
27. Greenberg RS, Long HK, Swigut T, and Wysocka J (2019). Single Amino Acid Change Underlies Distinct Roles of H2A.Z Subtypes in Human Syndrome. Cell 178, 1421–1436 e1424. 10.1016/j.cell.2019.08.002. [PubMed: 31491386]
28. Faast R, Thonglairoam V, Schulz TC, Beall J, Wells JR, Taylor H, Matthaei K, Rathjen PD, Tremethick DJ, and Lyons I (2001). Histone variant H2A.Z is required for early mammalian development. Curr Biol 11, 1183–1187. 10.1016/s0960-9822(01)00329-3. [PubMed: 11516949]
29. Giaimo BD, Ferrante F, Herchenrother A, Hake SB, and Borggrefe T (2019). The histone variant H2A.Z in gene regulation. Epigenetics Chromatin 12, 37. 10.1186/s13072-019-0274-9. [PubMed: 31200754]
30. Ye B, Yang L, Qian G, Liu B, Zhu X, Zhu P, Ma J, Xie W, Li H, Lu T, et al. (2020). The chromatin remodeler SRCAP promotes self-renewal of intestinal stem cells. EMBO J 39, e103786. 10.15252/embj.2019103786. [PubMed: 32449550]
31. Chauhan S, and Boyd DD (2012). Regulation of u-PAR gene expression by H2A.Z is modulated by the MEK-ERK/AP-1 pathway. Nucleic Acids Res 40, 600–613. 10.1093/nar/gkr725. [PubMed: 21937508]
32. Gallant-Behm CL, Ramsey MR, Bensard CL, Nojek I, Tran J, Liu M, Ellisen LW, and Espinosa JM (2012). DeltaNp63alpha represses anti-proliferative genes via H2A.Z deposition. Genes Dev 26, 2325–2336. 10.1101/gad.198069.112. [PubMed: 23019126]
33. Zovkic IB, Paulukaitis BS, Day JJ, Etikala DM, and Sweatt JD (2014). Histone H2A.Z subunit exchange controls consolidation of recent and remote memory. Nature 515, 582–586. 10.1038/nature13707. [PubMed: 25219850]
34. Cole L, Kurscheid S, Nekrasov M, Domaschenz R, Vera DL, Dennis JH, and Tremethick DJ (2021). Multiple roles of H2A.Z in regulating promoter chromatin architecture in human cells. Nat Commun 12, 2524. 10.1038/s41467-021-22688-x. [PubMed: 33953180]
35. Dong S, Han J, Chen H, Liu T, Huen MSY, Yang Y, Guo C, and Huang J (2014). The human SRCAP chromatin remodeling complex promotes DNA-end resection. Curr Biol 24, 2097–2110. 10.1016/j.cub.2014.07.081. [PubMed: 25176633]
36. Jahn N, Terzer T, Strang E, Dolnik A, Cocciardi S, Panina E, Corbacioglu A, Herzig J, Weber D, Schrade A, et al. (2020). Genomic heterogeneity in core-binding factor acute myeloid leukemia and its clinical implication. Blood Adv 4, 6342–6352. 10.1182/bloodadvances.2020002673. [PubMed: 33351131]
37. Tyner JW, Tognon CE, Bottomly D, Wilmot B, Kurtz SE, Savage SL, Long N, Schultz AR, Traer E, Abel M, et al. (2018). Functional genomic landscape of acute myeloid leukaemia. Nature 562, 526–531. 10.1038/s41586-018-0623-z. [PubMed: 30333627]

38. Knisbacher BA, Lin Z, Hahn CK, Nadeu F, Duran-Ferrer M, Stevenson KE, Tausch E, Delgado J, Barbera-Mourelle A, Taylor-Weiner A, et al. (2022). Molecular map of chronic lymphocytic leukemia and its impact on outcome. Nat Genet 54, 1664–1674. 10.1038/s41588-022-01140-w. [PubMed: 35927489]
39. Miller PG, Gibson CJ, Mehta A, Sperling AS, Frederick DT, Manos MP, Miao B, Hacohen N, Hodi FS, Boland GM, and Ebert BL (2020). Fitness Landscape of Clonal Hematopoiesis Under Selective Pressure of Immune Checkpoint Blockade. JCO Precis Oncol 4. 10.1200/PO.20.00186.
40. Gibson et al. (2023). Clonal Hematopoiesis in Young Women Treated for Breast Cancer. Clinical Cancer Research.
41. Weinstock DM, Nakanishi K, Helgadottir HR, and Jasin M (2006). Assaying double-strand break repair pathway choice in mammalian cells using a targeted endonuclease or the RAG recombinase. Methods Enzymol 409, 524–540. 10.1016/S0076-6879(05)09031-2. [PubMed: 16793422]
42. Heng TS, Painter MW, and Immunological Genome Project C (2008). The Immunological Genome Project: networks of gene expression in immune cells. Nat Immunol 9, 1091–1094. 10.1038/ni1008-1091. [PubMed: 18800157]
43. Ortmann CA, Dorsheimer L, Abou-El-Ardat K, Hoffrichter J, Assmus B, Bonig H, Scholz A, Pfeifer H, Martin H, Schmid T, et al. (2019). Functional Dominance of CHIP-Mutated Hematopoietic Stem Cells in Patients Undergoing Autologous Transplantation. Cell Rep 27, 2022–2028 e2023. 10.1016/j.celrep.2019.04.064. [PubMed: 31091442]
44. Wong MM, Cox LK, and Chrivia JC (2007). The chromatin remodeling protein, SRCAP, is critical for deposition of the histone variant H2A.Z at promoters. J Biol Chem 282, 26132–26139. 10.1074/jbc.M703418200. [PubMed: 17617668]
45. Cuadrado A, Corrado N, Perdiguero E, Lafarga V, Munoz-Canoves P, and Nebreda AR (2010). Essential role of p18Hamlet/SRCAP-mediated histone H2A.Z chromatin incorporation in muscle differentiation. EMBO J 29, 2014–2025. 10.1038/emboj.2010.85. [PubMed: 20473270]
46. Moran-Crusio K, Reavie L, Shih A, Abdel-Wahab O, Ndiaye-Lobry D, Lobry C, Figueroa ME, Vasanthakumar A, Patel J, Zhao X, et al. (2011). Tet2 loss leads to increased hematopoietic stem cell self-renewal and myeloid transformation. Cancer Cell 20, 11–24. 10.1016/j.ccr.2011.06.001. [PubMed: 21723200]
47. Loberg MA, Bell RK, Goodwin LO, Eudy E, Miles LA, SanMiguel JM, Young K, Bergstrom DE, Levine RL, Schneider RK, and Trowbridge JJ (2019). Sequentially inducible mouse models reveal that Npm1 mutation causes malignant transformation of Dnmt3a-mutant clonal hematopoiesis. Leukemia 33, 1635–1649. 10.1038/s41375-018-0368-6. [PubMed: 30692594]
48. Stavnezer J, Guikema JE, and Schrader CE (2008). Mechanism and regulation of class switch recombination. Annu Rev Immunol 26, 261–292. 10.1146/annurev.immunol.26.021607.090248. [PubMed: 18370922]
49. von Beck K, von Beck T, Ferrell PB Jr., Bick AG, and Kishtagari A (2023). Lymphoid clonal hematopoiesis: implications for malignancy, immunity, and treatment. Blood Cancer J 13, 5. 10.1038/s41408-022-00773-8. [PubMed: 36599826]
50. Horton SJ, Giotopoulos G, Yun H, Vohra S, Sheppard O, Bashford-Rogers R, Rashid M, Clipson A, Chan WI, Sasca D, et al. (2017). Early loss of Crebbp confers malignant stem cell properties on lymphoid progenitors. Nat Cell Biol 19, 1093–1104. 10.1038/ncb3597. [PubMed: 28825697]
51. Monroy MA, Schott NM, Cox L, Chen JD, Ruh M, and Chrivia JC (2003). SNF2-related CBP activator protein (SRCAP) functions as a coactivator of steroid receptor-mediated transcription through synergistic interactions with CARM-1 and GRIP-1. Mol Endocrinol 17, 2519–2528. 10.1210/me.2003-0208. [PubMed: 14500758]
52. Bosire R, Fadel L, Mocsar G, Nanasi P Jr., Sen P, Sharma AK, Naseem MU, Kovacs A, Kugel J, Kroemer G, et al. (2022). Doxorubicin impacts chromatin binding of HMGB1, Histone H1 and retinoic acid receptor. Sci Rep 12, 8087. 10.1038/s41598-022-11994-z. [PubMed: 35577872]
53. Wang X, Yan J, Shen B, and Wei G (2021). Integrated Chromatin Accessibility and Transcriptome Landscapes of Doxorubicin-Resistant Breast Cancer Cells. Front Cell Dev Biol 9, 708066. 10.3389/fcell.2021.708066. [PubMed: 34395436]

54. Soraas A, Matsuyama M, de Lima M, Wald D, Buechner J, Gedde-Dahl T, Soraas CL, Chen B, Ferrucci L, Dahl JA, et al. (2019). Epigenetic age is a cell-intrinsic property in transplanted human hematopoietic cells. Aging Cell 18, e12897. 10.1111/acel.12897. [PubMed: 30712319]
55. Zilberman D, Coleman-Derr D, Ballinger T, and Henikoff S (2008). Histone H2A.Z and DNA methylation are mutually antagonistic chromatin marks. Nature 456, 125–129. 10.1038/nature07324. [PubMed: 18815594]
56. Kamphuis P, van Zeventer IA, de Graaf AO, Salzbrunn JB, van Bergen M, Dinmohamed AG, van der Reijden BA, Schuringa JJ, Jansen JH, and Huls G (2023). Sex Differences in the Spectrum of Clonal Hematopoiesis. Hemasphere 7, e832. 10.1097/HS9.0000000000000832. [PubMed: 36713353]
57. Stirling DR, Swain-Bowden MJ, Lucas AM, Carpenter AE, Cimini BA, and Goodman A (2021). CellProfiler 4: improvements in speed, utility and usability. BMC Bioinformatics 22, 433. 10.1186/s12859-021-04344-9. [PubMed: 34507520]
58. Dobin A, Davis CA, Schlesinger F, Drenkow J, Zaleski C, Jha S, Batut P, Chaisson M, and Gingeras TR (2013). STAR: ultrafast universal RNA-seq aligner. Bioinformatics 29, 15–21. 10.1093/bioinformatics/bts635. [PubMed: 23104886]
59. Langmead B, and Salzberg SL (2012). Fast gapped-read alignment with Bowtie 2. Nat Methods 9, 357–359. 10.1038/nmeth.1923. [PubMed: 22388286]
60. Zhang Y, Liu T, Meyer CA, Eeckhoute J, Johnson DS, Bernstein BE, Nusbaum C, Myers RM, Brown M, Li W, and Liu XS (2008). Model-based analysis of ChIP-Seq (MACS). Genome Biol 9, R137. 10.1186/gb-2008-9-9-r137. [PubMed: 18798982]
61. Bailey TL, Boden M, Buske FA, Frith M, Grant CE, Clementi L, Ren J, Li WW, and Noble WS (2009). MEME SUITE: tools for motif discovery and searching. Nucleic Acids Res 37, W202–208. 10.1093/nar/gkp335. [PubMed: 19458158]
62. Ramirez F, Dundar F, Diehl S, Gruning BA, and Manke T (2014). deepTools: a flexible platform for exploring deep-sequencing data. Nucleic Acids Res 42, W187–191. 10.1093/nar/gku365. [PubMed: 24799436]
63. Li H, Handsaker B, Wysoker A, Fennell T, Ruan J, Homer N, Marth G, Abecasis G, Durbin R, and Genome Project Data Processing, S. (2009). The Sequence Alignment/Map format and SAMtools. Bioinformatics 25, 2078–2079. 10.1093/bioinformatics/btp352. [PubMed: 19505943]
64. Love MI, Huber W, and Anders S (2014). Moderated estimation of fold change and dispersion for RNA-seq data with DESeq2. Genome Biol 15, 550. 10.1186/s13059-014-0550-8. [PubMed: 25516281]
65. Hao Y, Hao S, Andersen-Nissen E, Mauck WM 3rd, Zheng S, Butler A, Lee MJ, Wilk AJ, Darby C, Zager M, et al. (2021). Integrated analysis of multimodal single-cell data. Cell 184, 3573–3587 e3529. 10.1016/j.cell.2021.04.048. [PubMed: 34062119]
66. Amezquita RA, Lun ATL, Becht E, Carey VJ, Carpp LN, Geistlinger L, Marini F, Rue-Albrecht K, Risso D, Soneson C, et al. (2020). Orchestrating single-cell analysis with Bioconductor. Nat Methods 17, 137–145. 10.1038/s41592-019-0654-x. [PubMed: 31792435]
67. Aran D, Looney AP, Liu L, Wu E, Fong V, Hsu A, Chak S, Naikawadi RP, Wolters PJ, Abate AR, et al. (2019). Reference-based analysis of lung single-cell sequencing reveals a transitional profibrotic macrophage. Nat Immunol 20, 163–172. 10.1038/s41590-018-0276-y. [PubMed: 30643263]
68. Sudlow C, Gallacher J, Allen N, Beral V, Burton P, Danesh J, Downey P, Elliott P, Green J, Landray M, et al. (2015). UK biobank: an open access resource for identifying the causes of a wide range of complex diseases of middle and old age. PLoS Med 12, e1001779. 10.1371/journal.pmed.1001779. [PubMed: 25826379]
69. Cibulskis K, Lawrence MS, Carter SL, Sivachenko A, Jaffe D, Sougnez C, Gabriel S, Meyerson M, Lander ES, and Getz G (2013). Sensitive detection of somatic point mutations in impure and heterogeneous cancer samples. Nat Biotechnol 31, 213–219. 10.1038/nbt.2514. [PubMed: 23396013]
70. Lek M, Karczewski KJ, Minikel EV, Samocha KE, Banks E, Fennell T, O'Donnell-Luria AH, Ware JS, Hill AJ, Cummings BB, et al. (2016). Analysis of protein-coding genetic variation in 60,706 humans. Nature 536, 285–291. 10.1038/nature19057. [PubMed: 27535533]

Highlights:

- *SRCAP* mutations in human clonal hematopoiesis are enriched in context of stress
- *Srcap* mutation enhances stem and progenitor cell function with a lymphoid bias
- Clonal advantage is manifest via augmented DNA repair and epigenetic regulation
- SRCAP represses the expression of DDR and HSC regulatory genes

A

Cohort	Patient type	# *SRCAP*	Tissue
Wong *et al.*[14]	Myeloma	4	Peripheral blood
	Lymphoma	27	
	Healthy donor	2	
DFCICAR[15]	Multiple myeloma or non-Hodgkin Lymphoma	27	Peripheral blood
Slavin *et al.*[24]	Multiple Myeloma	1	Peripheral blood
	non-Hodgkin Lymphoma	1	
	Healthy donor	1	
Beauchamp *et al.*[25]	Myelodysplastic syndromes (MDS)	12	Leukemia cells
	Non-cancer	53	Peripheral blood
CBF[36]	Acute myeloid leukemia (AML)	16	Leukemia cells
BEAT[37]	Acute myeloid leukemia (AML)	3	Leukemia cells
Knisbacher *et al.*[38]	Chronic lymphocytic leukemia (CLL)	14	Leukemia cells
Melanoma[39]	Melanoma	5	Peripheral blood
YWBC[40]	Breast cancer	8	Peripheral blood
MGB Biobank	Non-cancer	51	Peripheral blood
UK Biobank	Non-cancer	142	Peripheral blood

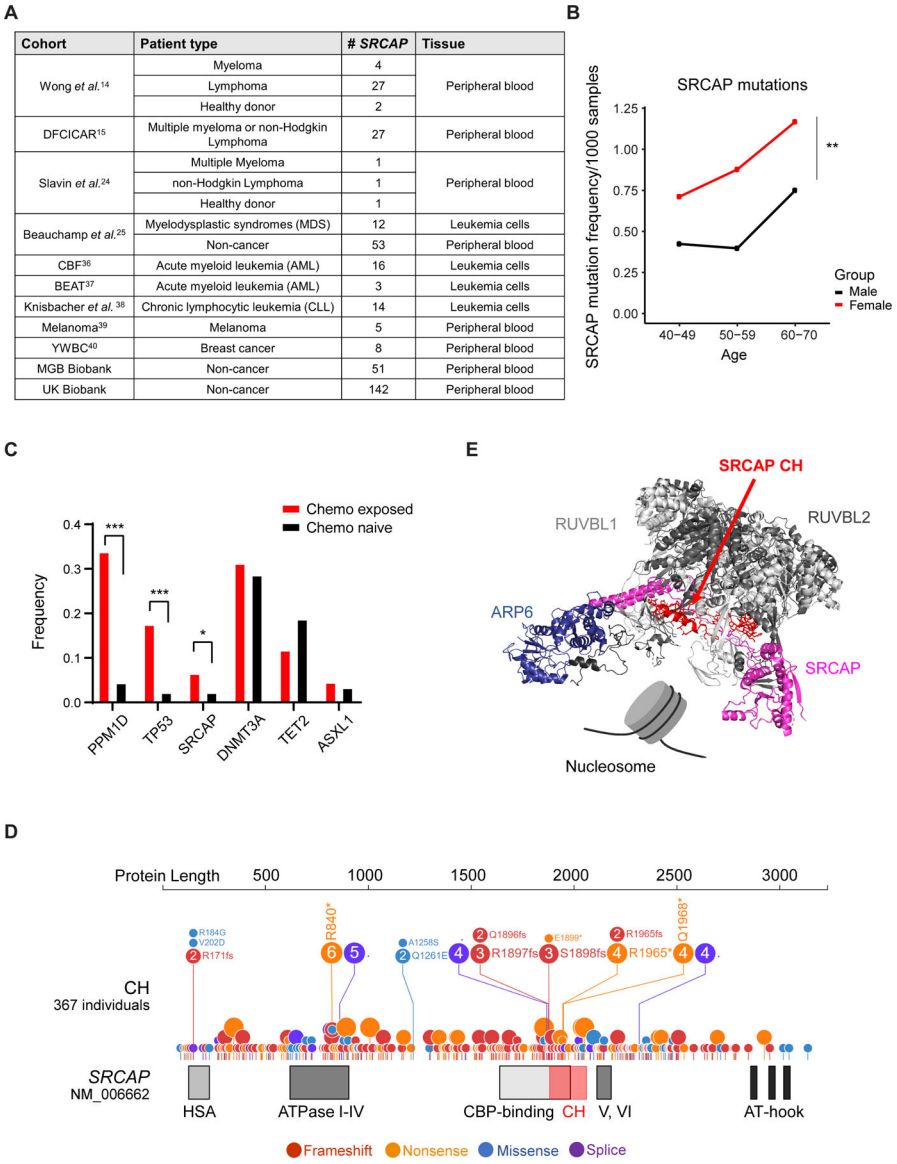

Figure1. CH-associated *SRCAP* mutations are enriched following exposure to genotoxic agents

(A) Characteristics of 367 individuals with *SRCAP* mutations. The patient cohort, disease type, number of cases with *SRCAP* mutations, and tissue sequenced are indicated. The MGB and UK Biobanks primarily include individuals without a known cancer diagnosis.

(B) Prevalence of *SRCAP* mutations in the UK Biobank. Males, n=46; females, n=95. Statistical significance determined by a multivariable logistic regression model adjusting for age and ever-smoked status.

(C) Frequency of mutations in recurrent CH genes in chemo-exposed (n=154) or a similar group of chemo-naïve patients (n=91). Cohorts were sequenced with the same NGS panel and have similar median age (63 vs 65 years). VAF threshold 0.01. Statistical significance determined by one-tailed *t*-test for the relative difference in proportions.

(D) Distribution of *SRCAP* mutations (n=367). Known functional domains and corresponding amino acids are indicated. The *SRCAP* CH-enriched region is labeled in red. The number of individuals with each mutation is indicated in the lollipops.
(E) Structure of the SRCAP complex (PDB 6IGM). SRCAP is highlighted in magenta with the *SRCAP* CH-enriched region in (D) labeled in red. Other proteins in the complex include RUVBL1 (light gray), RUVBL2 (dark gray), and ARP6 (Blue).
See also Table S1 and Figure S1.

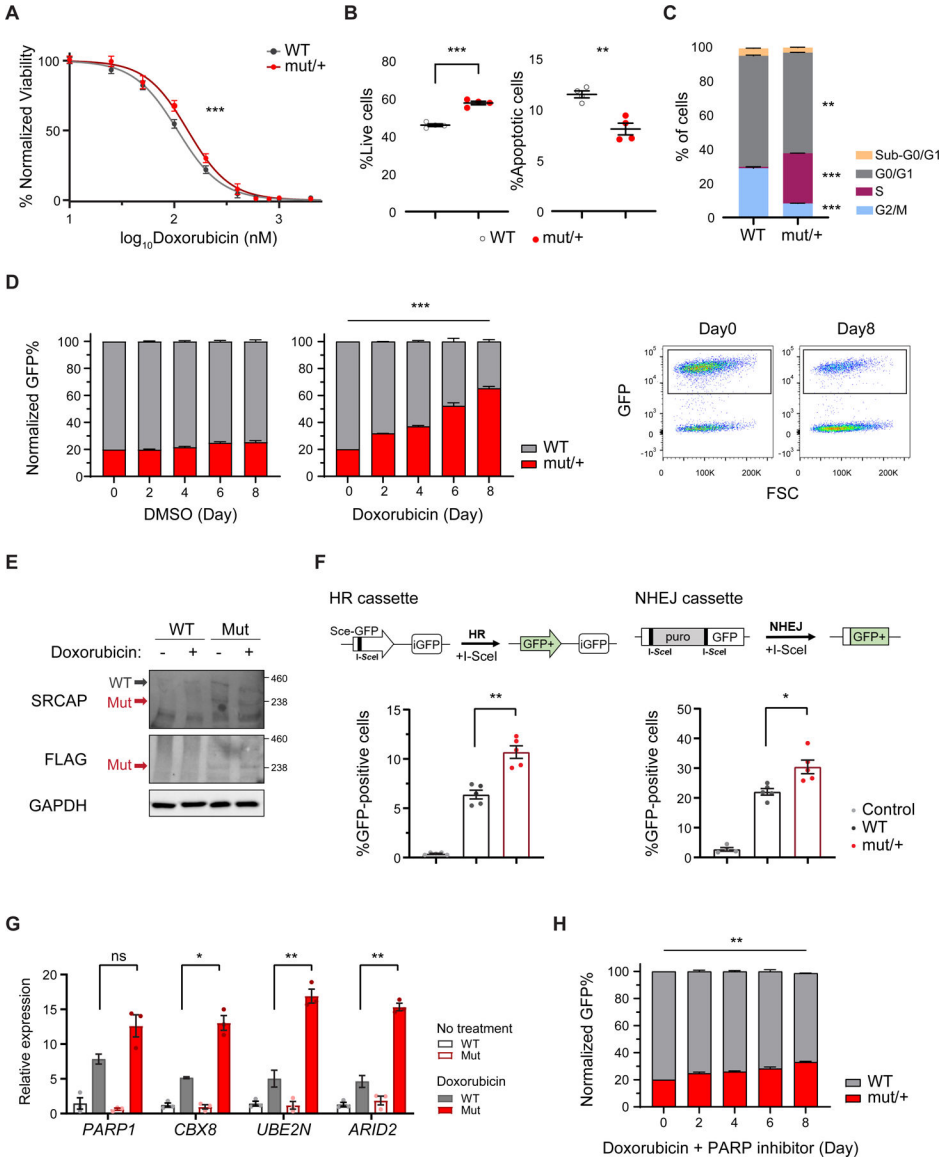

Figure 2. *SRCAP*$^{mut/+}$ cells exhibit enhanced DDR *in vitro* following genotoxic stress

(A) Dose-response with doxorubicin in WT and *SRCAP*$^{mut/+}$ MOLM-13 cells. Cell viability values were normalized to baseline (n=3). Statistical significance was determined by a non-linear regression modeling comparing LogIC50.

(B) Annexin V/7-AAD apoptosis with 120 nM (IC50) doxorubicin for 48 hr (n=4) and (C) BrdU/7-AAD cell cycle analysis with 100 nM (IC60) doxorubicin for 24 hr of WT and *SRCAP*$^{mut/+}$ MOLM-13 cells.

(D) *In vitro* competition of WT (GFP^{+}) and *SRCAP*$^{mut/+}$ (GFP^{-}) MOLM-13 cells with 60 nM (IC75) doxorubicin or DMSO. Left: proportion of WT and *SRCAP*$^{mut/+}$ cells measured by flow cytometry on indicated days (n=4). Right: representative flow plots. Data points are normalized to Day 0.

(E) WT and *Srcap*$^{mut/+}$ mouse embryonic fibroblasts (MEFs) cells treated with 200 nM (IC50) doxorubicin for 24 hr followed by western blot analysis probing with anti-SRCAP,

anti-FLAG and GAPDH. Endogenous SRCAP WT (3271 a.a.) and mutant (1963 a.a.) copies are highlighted with arrows.

(F) Top: schematic of the homologous recombination (HR) or non-homologous end joining (NHEJ) cassettes in U2OS cells. Gene-editing was performed on cells with integrated cassettes to generate isogenic WT and mutant clones. I-SceI digestion sites are shown in solid bars and GFP expression in green. Bottom: DNA repair via HR or NHEJ measured as percentages of GFP-positive cells in WT or *SRCAP*$^{mut/+}$ cells after I-SceI digestion (n=5) along with non-digested controls.

(G) Relative RNA expression levels of WT and *SRCAP*$^{mut/+}$ human MOLM-13 cells lines with or without doxorubicin (120 nM) for 24 hr.

(H) *In vitro* competition of WT (GFP^{+}) and *SRCAP*$^{mut/+}$ (GFP^{-}) MOLM-13 cells in the presence of 60 nM doxorubicin and 2 nM PARP inhibitor (Pamiparib). Proportion of WT and *SRCAP*$^{mut/+}$ cells measured by flow cytometry (n=3). All data points are normalized to Day 0.

Statistical significance was determined by unpaired two-tailed *t*-test (with Welch correction). All data represent mean ± SEM.

See also Figure S2.

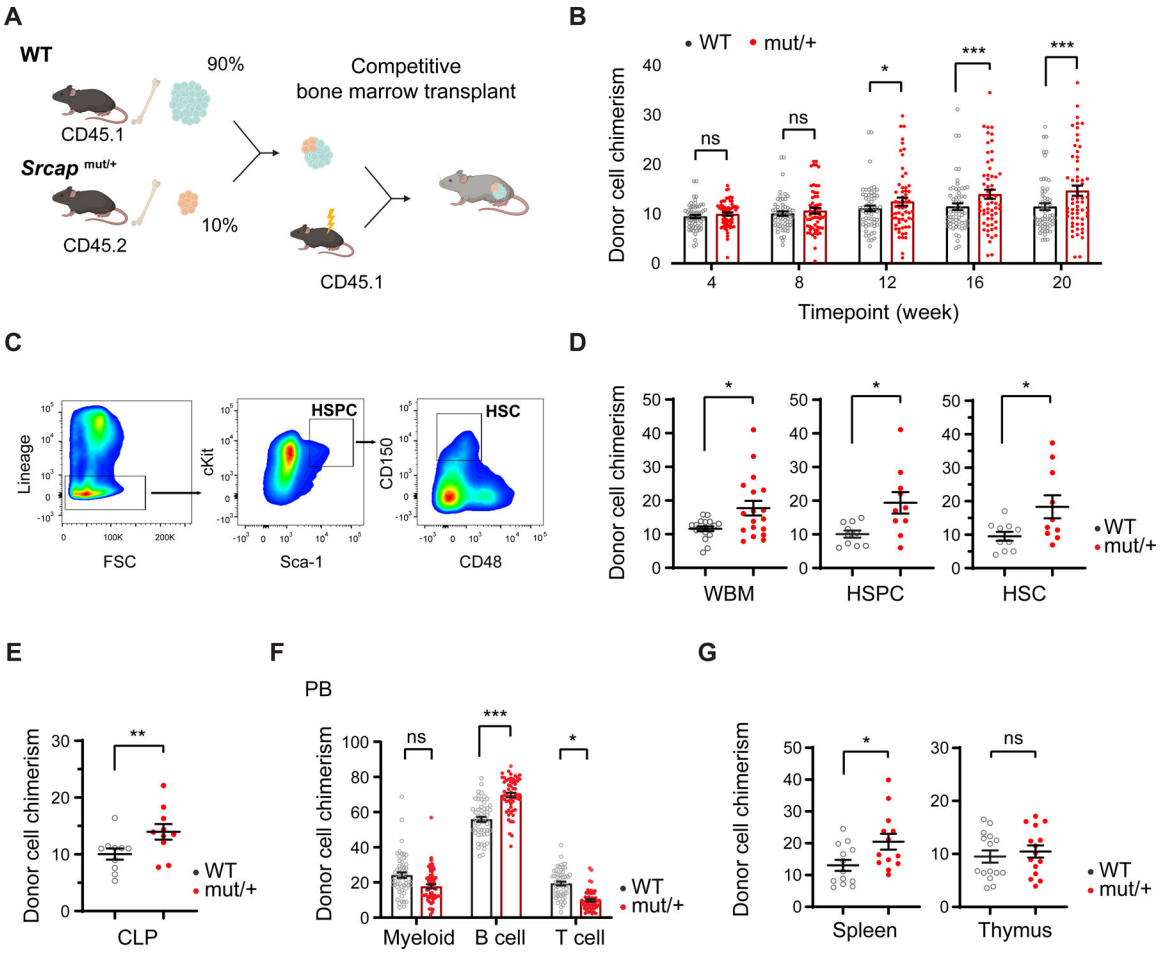

Figure 3. *Srcap* mutation leads to HSC expansion and lymphoid-biased hematopoiesis

(A) Murine competitive transplantation workflow. Whole bone marrow (WBM) was harvested from donor CD45.2 *Srcap*$^{mut/+}$ and CD45.1 WT (blue) mice, mixed at a 10:90 ratio, and transplanted to lethally irradiated CD45.1 recipients. Mice were bled every 4 weeks to analyze the contribution of test cells. A parallel transplant competed WT (CD45.2) against WT (CD45.1) cells serves as the WT:WT control cohort.

(B) Test cell (CD45.2) chimerism in the peripheral blood of recipients in (A) (n=60). *Srcap*$^{mut/+}$ cohort is depicted in red and the parallel WT:WT control cohort in gray.

(C) Representative flow plots depicting the gating strategy for HSPC and HSC.

(D-G) Recipient mice in (B) were sacrificed at 20 weeks post-transplantation, and the contributions of test cells were assessed in (D) WBM (n=18), HSPC (n=10), and HSC populations (n=10), (E) common lymphoid progenitors (CLP) (n=10), (F) myeloid, B-cell, T-cell lineages in peripheral blood (n=58), and (G) spleen (n=14) and thymus (n=14). The *Srcap*$^{mut/+}$ cohort is indicated in red, and the parallel WT:WT cohort in gray.

Statistical significance was determined by unpaired two-tailed *t*-test (with Welch correction). All data represent mean ± SEM with individual values.

See also Figure S3 and Table S3.

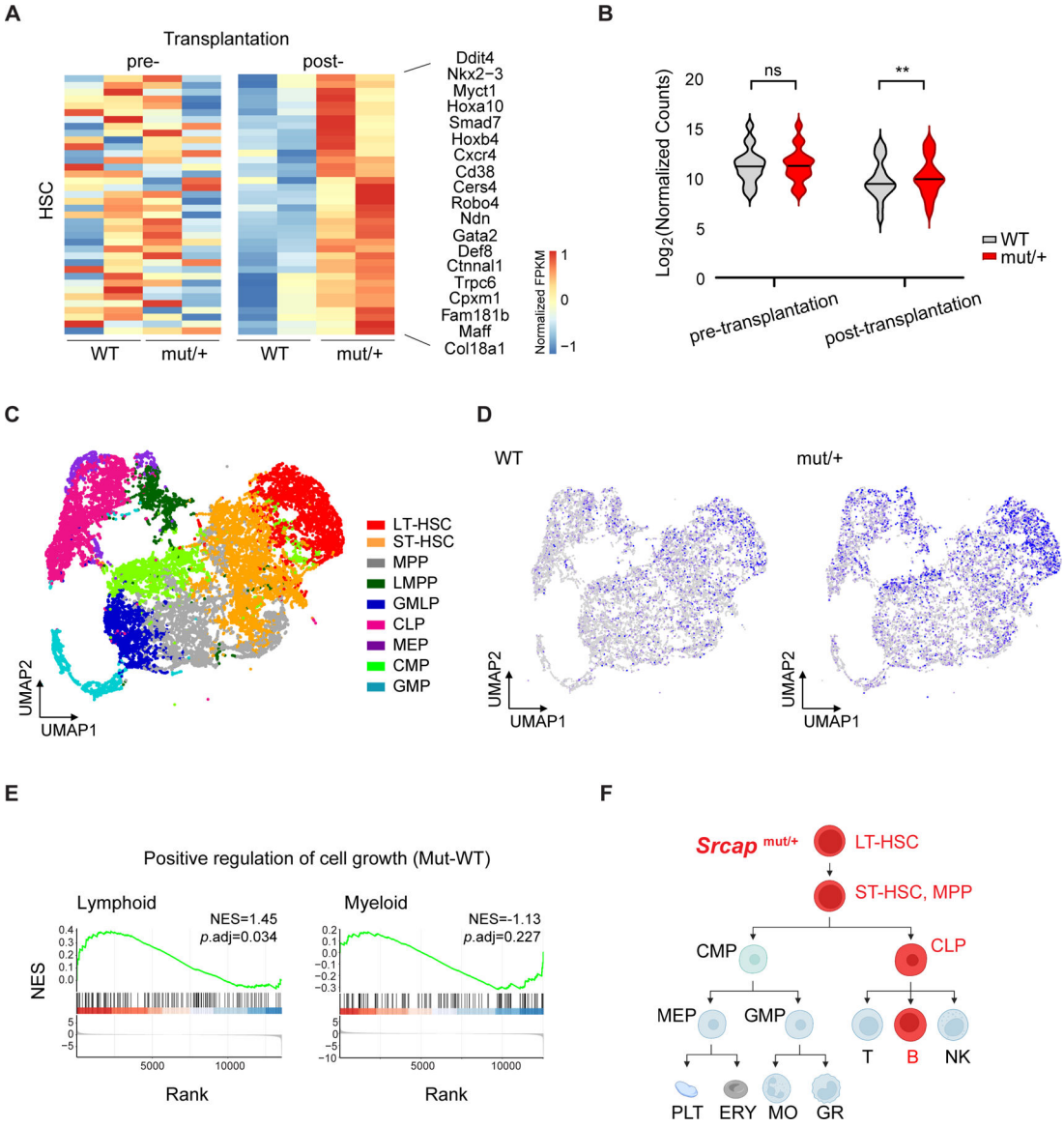

Figure 4. Transcriptomic regulation of *Srcap* mutant lymphoid-biased expansion

(A) Relative gene expression from RNA-sequencing of HSPCs before and after competitive transplantation as in Figure 3A. Test cells (CD45.2) were isolated from the *Srcap*$^{mut/+}$:WT and the WT:WT cohorts. The gene set displayed includes genes highly expressed in HSCs (Immunological Genome Project).[42] Statistical significance determined by DESeq2 with duplicates.

(B) Normalized read counts assigned to genes (n=36). Statistical significance determined by Mann-Whitney *U*-test.

(C) Single-cell RNA-seq of HSPCs 20 weeks after competitive. UMAP clustering colored by cell types: long-term HSCs (LT-HSCs), short-term HSCs (ST-HSCs), multipotent progenitors (MPPs), lymphoid-primed multipotent progenitors (LMPPs), granulocyte/monocyte/lymphoid progenitors (GMLPs), common lymphoid progenitors

(CLPs), megakaryocyte-erythrocyte progenitors (MEPs), common myeloid progenitors (CMPs), and granulocyte-macrophage progenitors (GMPs).

(D) Single-cell RNA-seq UMAP colored by the *Srcap*$^{mut/+}$ signature. Gene signature scores are extracted based on top differentially expressed genes ($p<0.05$) in the lymphoid clusters determined by Mann-Whitney U statistics. The color is scaled to maximum score in blue and minimum score in gray. Feature plots separated by genotype are shown.

(E) Gene set enrichment analysis (GSEA) of *Srcap*$^{mut/+}$ lymphoid and myeloid clusters compared to WT counterparts for the gene set '*positive regulation of cell growth*' (GO:0045787). Normalized enrichment score (NES) and adjusted *p*-value are indicated.

(F) Depiction of the cell populations (red) affected by *Srcap*$^{mut/+}$ mutation in our mouse model.

See also Figure S4.

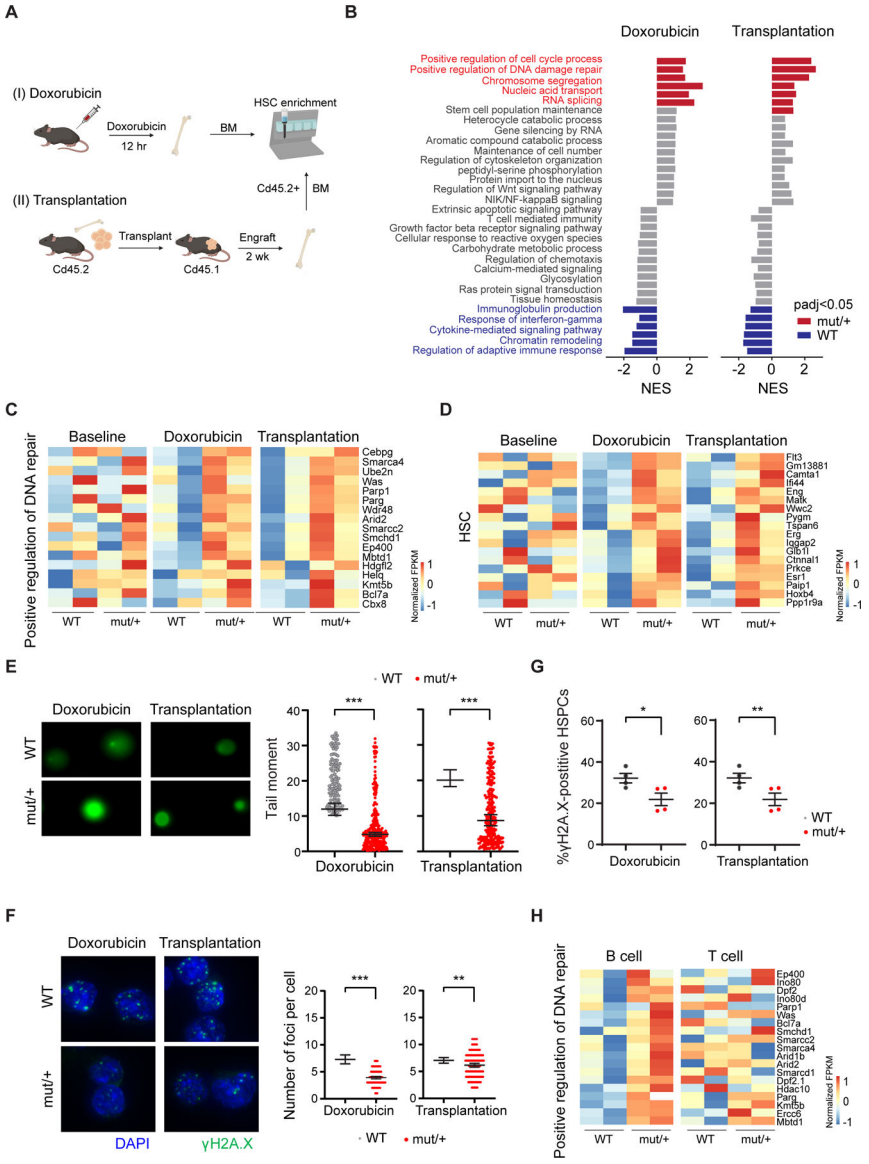

Figure 5. Doxorubicin and transplantation are stressors promoting *Srcap*$^{mut/+}$ advantage

(A) Schematic to study doxorubicin and transplantation as cellular stressors. Doxorubicin: mice were intraperitoneally injected with one dose of 10 mg/kg doxorubicin, and bone marrow was harvested after 12 hr. Transplantation: *Srcap*$^{mut/+}$ or WT cells were transplanted non-competitively into lethally irradiated recipients and then isolated from bone marrow after 2 weeks followed by enrichment and/or sorting for HSPCs.

(B) GSEA plot of *Srcap*$^{mut/+}$ HSPCs after doxorubicin or transplantation. Red and blue bars indicate significantly up- and down-regulated pathways. Normalized enrichment score (NES) and adjusted *p*-value < 0.05 are indicated.

(C-D) Relative gene expression from RNA-sequencing of HSPCs at baseline or after stress showing normalized read counts of (C) the gene set "*positive regulation of DNA repair*" (GO: GO:0045739) (D) genes typically enriched in HSC.[42] Statistical significance determined by DESeq2 with duplicates.

(E-F) HSC-enriched bone marrow cells with stress were used for (E) comet assay showing the amount of DNA damage (left: representative comet microscopy image; right: quantification of tail moment) and (F) γH2A.X foci analysis (left: representative immunofluorescence microscopy images; right: number of γH2A.X foci per cell). Statistical significance was determined by Mann-Whitney *U*-test. Data represent mean ± 95% confidence interval (n=256 each group).

(G)Percentage of γH2A.X-positive WT or *Srcap*$^{mut/+}$ HSPCs with doxorubicin (n=4) or after transplantation (n=5). Statistical significance was determined by unpaired two-tailed *t*-test (with Welch correction). Data represent mean ± SEM.

(H) Relative gene expression from RNA-sequencing of bone marrow-derived B- and T-cells at baseline and after stress showing normalized read counts of genes in the gene set "*positive regulation of DNA repair*". Statistical significance determined by DESeq2 with duplicates. See also Figure S5.

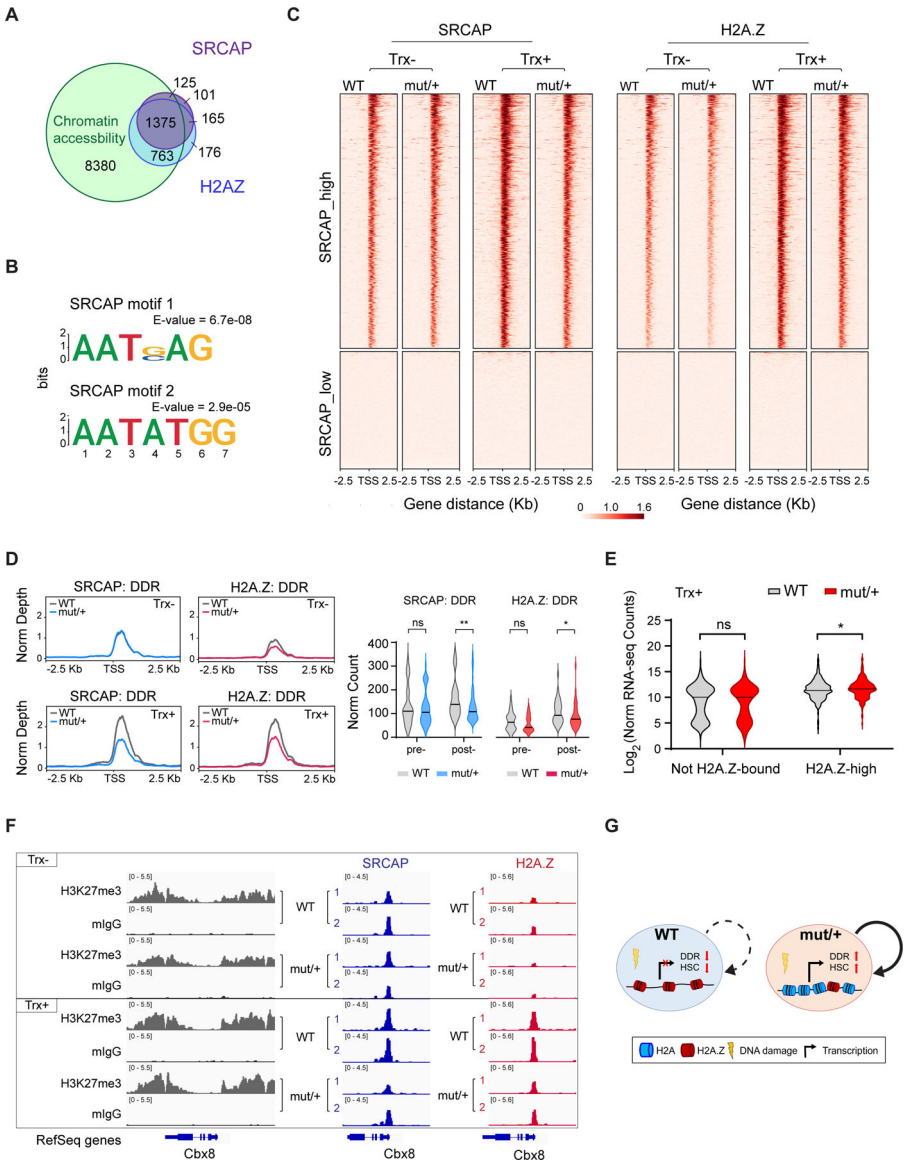

Figure 6. Decreased chromatin remodeling in *Srcap*$^{mut/+}$ stem cells after stress

(A) Venn diagram of TSS-promoter peaks from ATAC-sequencing and CUT&RUN for SRCAP and H2A.Z of WT HSPCs after 12 weeks of competitive transplantation. Numbers of overlapping peaks are indicated.

(B) Multiple Em for Motif Elicitation (MEME) analysis of SRCAP localization at the TSS-promoter. Top two motifs and *E*-value are shown.

(C) Enrichment of SRCAP and H2A.Z at TSS-promoter before and after competitive transplantation. Enrichment at the clustered regions based on high and low SRCAP abundance is shown.

(D) Average density of mapped reads (left) and normalized read count (right) of HSPCs were before or after 12 weeks of competitive transplantation. SRCAP and H2A.Z signals centered to TSS of genes in the gene set "*positive regulation of DNA repair*" (GO:

GO:0045739). Statistical significance determined by Mann-Whitney *U*-test. Mean and *p*-value are shown.

(E) Multi-omics integration of normalized RNA-seq read counts of CD45.2 HSPCs 12 weeks after transplantation. H2A.Z-high and not H2A.Z-bound genes are determined by CUT&RUN as in (C).

(F) Integrative Genomic Viewer (IGV) browser tracks for SRCAP (blue) and H2A.Z (red) enrichment at *Cbx8* (mm10, chr11:119,036,305–119,040,969) in the HSPCs before or after competitive transplantation. H3K27me3 and mIgG enrichment tracks for each condition are shown as positive and negative controls.

(G) Diagram depicting the epigenetic and transcriptomic regulation of $Srcap^{mut/+}$ cells with exposure to stressors. The circular arrows denote stem cell survival under stress and proliferation.

See also Figure S6.

~~KEY RESOURCE TABLE~~

REAGENT or RESOURCE	SOURCE	IDENTIFIER
Antibodies		
PE-Cy7 anti-Mouse Ly-6G	eBioscience	25–5931-82
PE-Cy7 anti-Mouse CD11b	BD Bioscience	552850
PE-Cy7 anti-Mouse B220	BD Bioscience	552772
eFluor 450 anti-Mouse CD4	eBioscience	48–0042-82
eFluor 450 anti-Mouse CD8a	eBioscience	48–0081-82
eFluor 450 anti-Mouse B220	eBioscience	48–0452-82
eFluor 450 anti-Mouse TER-119	eBioscience	48–5921-82
APC-Cy7 anti-Mouse CD117	BioLegend	135136
PE-Cy7 anti-Mouse Sca-1	eBioscience	25–5981-82
BV510 anti-mouse CD48	BD Bioscience	563536
PE anti-Mouse CD150	eBioscience	12–1502-82
APC anti-Mouse CD45.1	eBioscience	17–0453-82
FITC anti-Mouse CD45.2	eBioscience	11–0454-82
PE anti-Mouse CD16/32	eBioscience	12–0161-82
FITC anti-Mouse CD127	eBioscience	11–1271-82
PB anti-Mouse CD45.2	eBioscience	48–0454-82
APC anti-Mouse CD34	BioLegend	119309
Mouse monoclonal M2 anti-FLAG	Sigma Aldrich	F1804–200UG
Rabbit monoclonal phospho-Histone H2A.X (Ser139)	Cell Signaling	9718S
Alexa Fluor® 647 AffiniPure Donkey Anti-Rabbit IgG (H+L)	Jackson Immuno	711–605-152
Alexa Fluor® 488 AffiniPure Goat Anti-Mouse IgG (H+L)	Jackson Immuno	115–545-062
Alexa Fluor® 488 AffiniPure Donkey Anti-Rabbit IgG (H+L)	Jackson Immuno	711–545-152
FITC anti-mouse Phospho H2A.X Phospho (Ser139)	BioLegend	613403
Rabbit monoclonal anti-H3K27me3	Cell Signaling	9733S
Rabbit polyclonal anti-IgG	Abcam	ab46540
Rabbit polyclonal anti-SRCAP	Kerafast	ESL103
Rabbit monoclonal anti-H2A.Z	Cell Signaling	50722S
Chemicals, peptides, and recombinant proteins		
Doxorubicin	Selleck	S1208
Etoposide	Selleck	S1225
Cytarabine	MedChemExpress	HY-13605
Daunorubicin	Selleck	S3035
Pamiparib	MedChemExpress	1446261–44-4
DAPI	Sigma Aldrich	D8417
Mouse CD117 MicroBeads	Miltenyi	130–091-224
Digtonin	Promega	G9441

REAGENT or RESOURCE	SOURCE	IDENTIFIER
Concanavalin-coated Magnetic Beads	Bangs Laboratories	BP531
cOmplete™, EDTA-free Protease Inhibitor Cocktail	Sigma Aldrich	11873580001
CUTANA® pAG-MNase	EpiCypher	15–1016
Critical commercial assays		
AllPrep DNA/RNA Micro Kit	Qiagen	80284
Cell Proliferation Kit I	Sigma Aldrich	11465007001
FITC BrdU Flow Kit	BD Bioscience	559619
FITC Annexin V Apoptosis Detection Kit I	BD Bioscience	556547
TruSeq® Stranded mRNA Library Prep	Illumina	20020594
CUTANA™ DNA Purification Kit	EpiCypher	14–0050
NEBNext® Ultra™ II DNA Library Prep Kit for Illumina	New England Biolabs	E7645
Nextera XT DNA Library Preparation Kit	Illumina	FC-131–1096
DNA Clean & Concentrator	Zymo Research	D4030
Deposited data		
RNA-sequencing data	This paper	GEO #GSE230155
Single cell RNA-seq data	This paper	GEO #GSE230155
CUT&RUN data	This paper	GEO #GSE230155
ATAC-sequencing data	This paper	GEO #GSE230155
Experimental models: Cell lines		
MOLM-13 WT	DSMZ	Cat# ACC-554
MOLM-13 SRCAPQ$^{1963X/+}$	This paper	N/A
Lenti-X™ 293T WT	Takara	632180
Lenti-X™ 293T SRCAPQ$^{1963XI+}$	This paper	N/A
U-2 OS HR reporter WT	Bertuch Lab[41]	N/A
U-2 OS HR reporter	This paper	N/A
U-2 OS NHEJ reporter WT	Bertuch Lab[41]	N/A
U-2 OS NHEJ reporter SRCAPQ$^{1963X/+}$	This paper	N/A
Experimental models: Organisms/strains		
Mice: Srcap$^{Q1963X/+}$	This paper	N/A
Mice: C57BL6/J	Jackson Laboratory	Stock #000664
Mice: CD45.1 (B6.SJL-Ptprc^{a}pepc^{b}/Boyj)	Jackson Laboratory	Stock #002014
Oligonucleotides		
Primers for cloning	See Table S2	N/A
Primers for genotyping	See Table S2	N/A
Recombinant DNA		
pCBASceI plasmid	Addgene	26477
Human SRCAP ORF Clone in Gateway Cloning Vector	Antibodies-online	ABIN3417640
sgRNAs for CRISPR	See Table S2	N/A
ssODNs for CRISPR	See Table S2	N/A

REAGENT or RESOURCE	SOURCE	IDENTIFIER
Software and algorithms		
Adobe Illustrator	Adobe	https://www.adobe.com/products/illustrator.html
SnapGene (v4.3.11)	Dotmatics	https://www.snapgene.com/
Comet Assay IV software	Instem	https://www.instem.com/solutions/genetic-toxicology/comet-assay.php
PRISM (v8.4.2)	GraphPad	https://www.graphpad.com/scientific-software/prism/
FACSdiva (v8.0.1)	BD Biosciences	https://www.bdbiosciences.com/en-eu/products/software/instrument-software/bd-facsdiva-software
FlowJo (v10.7.1)	BD Biosciences	https://www.flowjo.com/
CellProfiler (v4.2.1)	Stirling et al.[57]	https://cellprofiler.org/
Cell Ranger (v6.1.2)	10x Genomics	https://support.10xgenomics.com/single-cell-gene-expression/software/overview/welcome
bcl2fastq conversion software	Illumina	https://sapac.support.illumina.com/sequencing/sequencing_software/bcl2fastq-conversion-software.html
STAR (v020201)	Dobin et al.[58]	https://github.com/alexdobin/STAR
Bowtie2 (v2.2.8)	Langmead et al.[59]	https://bowtie-bio.sourceforge.net/bowtie2/index.shtml
MACS3 (v3.0.0a6)	Zhang et al.[60]	https://github.com/macs3-project/MACS
memes (v1.4.1)	Bailey et al.[61]	https://meme-suite.org/meme/
HOMER	UCSD	http://homer.ucsd.edu/homer/motif/
deepTools (v3.5.1)	Ramirez et al.[62]	https://deeptools.readthedocs.io/en/develop/
SAMTools (v0.1.19)	Li et al.[63]	http://www.htslib.org/
R (v4.2.0)	r-project	https://www.r-project.org/
DESeq2 (v1.36.0)	Love et al.[64]	https://bioconductor.org/packages/release/bioc/html/DESeq2.html
Seurat (v4.2.0)	Hao et al.[65]	https://satijalab.org/seurat/
SingleCellExperiment (v1.18.1)	Amezquita et al.[66]	https://github.com/drisso/SingleCellExperiment
SingleR (v1.10.0)	Aran et al.[67]	https://github.com/dviraran/SingleR
Integrative Genome Viewer	Broad Institute	https://software.broadinstitute.org/software/igv/
Other		
QuadroMACS	Miltenyi	130–091-051
LS Columns for QuadroMACS	Miltenyi	130–042-401
MethoCult GF	STEMCELL	3434
NEON Transfection System	ThermoFisher	N/A
High sensitivity D1000 ScreenTape	Agilent	5067–5584
D5000 ScreenTape	Agilent	5067–5588